CHALMERS

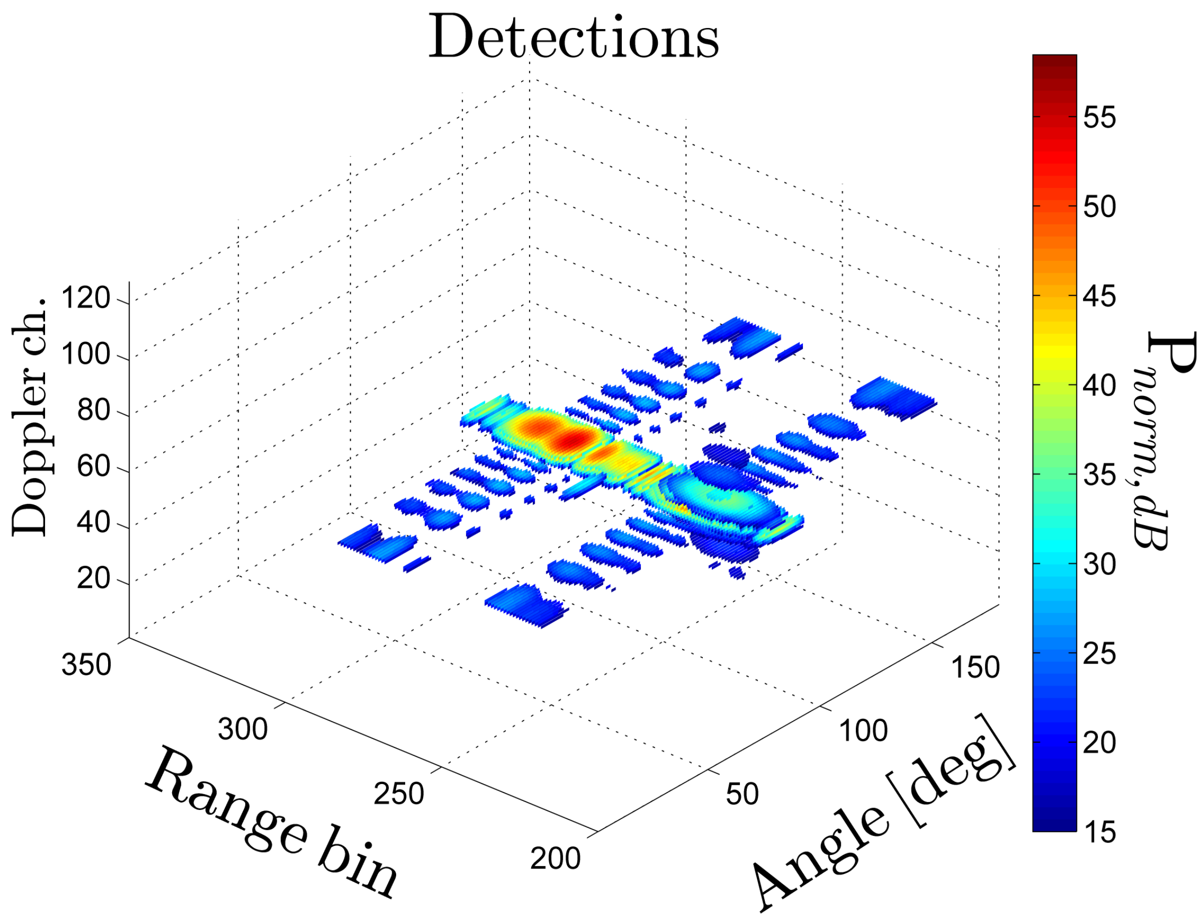

Modelling of Digital Radar

Master's thesis in Applied Physics

ALBIN JONASSON SVÄRDSBY

Department of Microtechnology and Nanoscience
CHALMERS UNIVERSITY OF TECHNOLOGY
Gothenburg, Sweden 2015

MASTER'S THESIS IN APPLIED PHYSICS

Modelling of Digital Radar

ALBIN JONASSON SVÄRDSBY

Department of Microtechnology and Nanoscience
CHALMERS UNIVERSITY OF TECHNOLOGY

Gothenburg, Sweden 2015

Modelling of Digital Radar
ALBIN JONASSON SVÄRDSBY

Master's thesis 2015:01XXXX
ISSN XXXX-XXXX
Department of Microtechnology and Nanoscience
Chalmers University of Technology
SE-412 96 Gothenburg
Sweden
Telephone:

Cover:

Chalmers Reproservice
Gothenburg, Sweden 2015

Modelling of Digital Radar
Master's thesis in Applied Physics
ALBIN JONASSON SVÄRDSBY
Department of Microtechnology and Nanoscience
Chalmers University of Technology

Abstract

The advances in modern electronics pave way for new ways to design radar systems. The existence of Analogue to Digital Converters (ADC) capable of sampling at GHz make it possible to sample the RF signal directly, removing the need for prior down mixing. This gives a possibility to design very simple receiver channels and move traditional operations from hardware to software. This greatly helps cutting cost of manufacturing and development and opens up for a very configurable system. This configurability comes at the cost of decreased selectivity, resulting in that external signals outside the radar system's signal bandwidth but inside the receiver band will become amplified as well, with the risk of saturating the amplifiers. Because of this it is interesting to study the impact of the non-linearities on detectability. The simple design of the system makes it feasible to simulate the full system chain from transmitter to signal processing after the receiver.

This thesis treats the methods used to create a model in order to simulate the operation and non-linear effects of a Uniform Linear Array (ULA) digital pulse doppler radar system from generation of transmission waveform to the signal processing of the sampled output from the receiver channels. The methods involve electronic simulations of amplifiers utilising a 5th degree polynomial and filtering and sampling processes. The thesis further features techniques used to enhance the Signal to Noise Ratio (SNR) of a desired signal from a phased array and position it in a 3D space with 2 room dimensions and 1 velocity dimension. The model is then utilised to study the effects of non-linear effects of the system when the input to the receiver is disturbed by a strong clutter signal or a strong external signal. The thesis also treats the effect on detectability of a target when an external signal give rise to higher order harmonics from amplifier saturation and clipping during sampling that then is folded into the radar system's final sampling band.

The thesis finds it feasible to perform full system simulations from waveform generation to detection and it is found that the non-linear effects due to strong disturbances negatively affect the desired target SNR and may in some cases be the source of false detections. The results is found by studying common radar cases, with varying input power to the receiver. The thesis finds that it is possible to digitally suppress external signals outside the final sampling band but the decrease in SNR for the desired signal, due to saturation of the radar system, still remains.

Keywords: Digital radar, doppler filter, RF sampling, non-linear amplifiers

Preface

The idea for this master thesis was developed at EDS, SAAB, Göteborg and the thesis has also been written i collaboration with SAAB.

Acknowledgements

The author would like to extends his thanks to the people at EDS, SAAB Göteborg for their help and advice. He would also like to thank Christian Fager at MC2, Chalmers for constructive feedback. A special thank is to be extended to Anders Silander for many constructive discussions and valuable feedback.

Abreviations and symbols

ADC	Analogue to Digital Converter
CNR	Clutter to Noise Ratio
CW	Continuous Wave
DAC	Digital to Analogue Converter
DSP	Digital Signal Processing
JNR	Jammer to Noise Ratio
P_{1dB}	1dB compression point
PRF	Pulse Repetition Frequency
RCS	Radar Cross Section
Rx	Reciever
SNR	Signal to Noise Ratio
SOI or IP_2	Second-order interception point
TOI or IP_3	Third-order interception point
Tx	Transmitter
ULA	Uniform Linear Array

Contents

1 Introduction

The advances in modern electronics pave way for new ways to design radar systems. The existence of Analogue to Digital Converters (ADC) capable of sampling at GHz make it possible to sample the RF signal directly. Traditionally this has not been feasible and the RF design usually consists of mixers to alter the carrier frequency of the signal allowing for sampling of the RF signal at a lower rate. In addition to this the process of down-mixing also includes filter operations in order to avoid aliases after sampling. This in turn increases the complexity of the RF construction, resulting in higher cost for components, manufacturing and development.

With digital radar you circumvent many of these steps by allowing the signal to be sampled directly without prior down-mixing. By directly letting the ADC sample the signal you transfer operations traditionally performed in the hardware to digital operations in software. The benefits of doing so is that you will get a more configurable system where software operations easier can be changed, allowing for customisation not traditionally allowed, at a reduced cost. The trade-off you get by moving these operations to software is that the system has a broader listening band, since it doesn't have the hardware filters normally placed together with the down-mixing. Since the system has a broader listening band it also becomes more sensitive to external signals, outside our signal bandwidth, which traditionally where filtered away during down-mixing. These external signals might then saturate the system and it is therefore interesting to study the effects of non-linearity on detectability.

Given that the complexity of the receiver design is greatly reduced the system basically becomes a set of transmitter and receiver channels, each consisting of a set of filters and amplifiers. By then sample each channel individually results in a very predictable and configurable system. This rather crude, yet elegantly simple and practical design makes it very viable to perform full system simulations, which is the purpose of this thesis.

1.1 Problem formulation

The purpose of the thesis is mainly to study the impact of non-linearity on sensitivity. The more specific problem formulation that constitute the foundation of the thesis can be divided into two parts, presented in 1.1.1 and 1.1.2.

1.1.1 Design a model for the radar system

The first part is to design a simulation model of the entire radar chain including generation of waveform to transmission, target interaction, receiver and signal processing. For the RF parts in the model factors of value are gain, dynamic range, noise factor and linearity. When looking at the whole system the most important factor is sensitivity.

1.1.2 Usage of Model

The second part of the problem formulation is to use the system to study cases consisting of 4 types of signals:

- Echo signal from a target, like an air plane.
- Strong echo signal from clutter, for example a hill.
- Deliberate noise disturbance, either within the radars transmission band or in close vicinity but still outside the transmission band.
- Interference signals from other transmitters, like another radar, both inside and outside our transmission band.

When constructing cases using the above signals, combinations of two should be prefered, with the goal to study the sensitivity of target detection. For example a case with one target in the presence of strong clutter that saturates the receiver.

1.2 Limitations of the thesis

The type of radar that this thesis will treat is a digital phased uniform linear array (ULA) radar designed for L-band, 1-2GHz, sending a linear chirp with 5MHz bandwidth and centre frequency 1.3GHz. The system consists of 13 elements equidistantly placed with half of a wavelength separation. A detection is defined in the thesis to when the signal to noise ration (SNR) is higher than or equal to 13dB.

The thesis will only treat the non-linearity that stem from the receiver and sampling of signals, meaning that the transmission chain is treated linearly. Neither will it treat situations when components reach breakdown region, it will always be assumed that a component will not break due to high input power. Further the thesis will not treat methods for tracking the target but will only focus on the strength of the signal and its SNR. Regarding simulations, all physical object will be treated as point object, although sometimes complemented with attributes such as area. During simulations effects due to coupling and other interactions between the different antennas and corresponding circuits are ignored.

2 Theory

In this chapter theory relevant to the modelling of a radar system is presented. Initially the basic design of a digital radar is presented and following this is the theory used to implement the different stages.

2.1 Radar system

In its essence, a radar system is a device which transmits an electromagnetic wave in the frequency range 3kHz-300GHz and listens to the returning echo of the wave after it interacts with an object. It typically consists of an electric generator of radio waves (transmitter or Tx) combined with a radiator of the waves (antenna) to emit the signal, and corresponding, a receiver of the radio waves (receiver or Rx), using an antenna to collect the incoming wave for signal operations as is basically showed in figure 2.1.

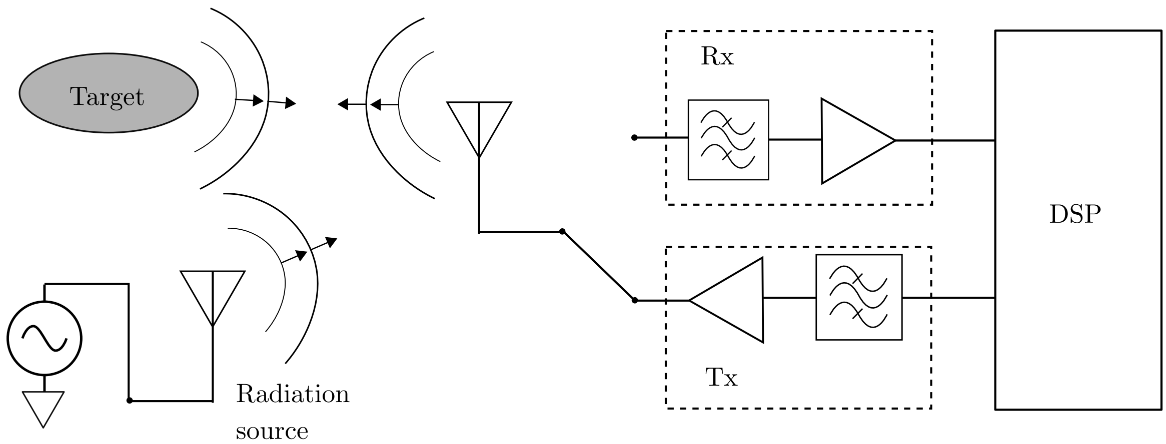

Figure 2.1: *The figure schematically shows the basic radar setup, with receiver (Rx) and transmitter (Tx) connected to an antenna. To the left is a target resulting in pulse echoes and a external transmitter generating a signal. To the right of the Tx and Rx there's a Digital Signal Processing (DSP) block, grouping together the generation of the signal for the Tx and the processing of the signal from Rx.*

For the case of digital radar we are generally interested in array of antennas, where each antenna has a corresponding Tx/Rx connection schematically shown in figure 2.2

When an incident wave centred round a centre frequency, f_c, has been collected by the antenna and reached the receiver the wave is amplified and filtered in order to extract the desired signal. Here digital radars has an advantage in that most processing takes placed digitally after the signal has been sampled and stored in digital form. This in turn lowers the requirements of the electronics in the receiver to basically be a series of amplifiers and filters so that the echo in the designed bandwidth is amplified while interference and noise outside of the frequency band of the filter is suppressed. This is also one of the biggest potential issues with

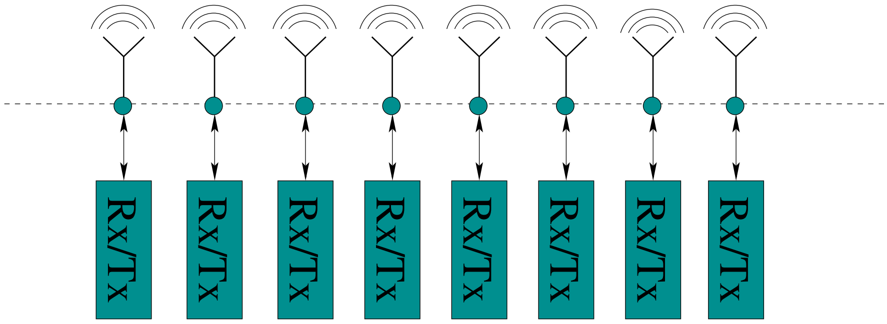

Figure 2.2: *The figure illustrate a line up of many antenna element in an ULA.*

a digital radar, since an external signal that still is within the receiver passband but outside our bandwidth of interest will be able to freely pass trough the receiver, being amplified in the process, and might therefore impact the results from the digital processing if it saturates the receiver. In the case of a traditional radar this problem is removed during the filter and down mixing in the receiver by successively narrowing the band.

Having amplified and filtered the signal we will treat the signal in order to determine the target's position in room space and radial velocity space as well as increasing the SNR. The different operations that will be performed is schematically showed in figure 2.3 where the different operations performed in the DSP block in figure 2.1 is presented for the receiver chain.

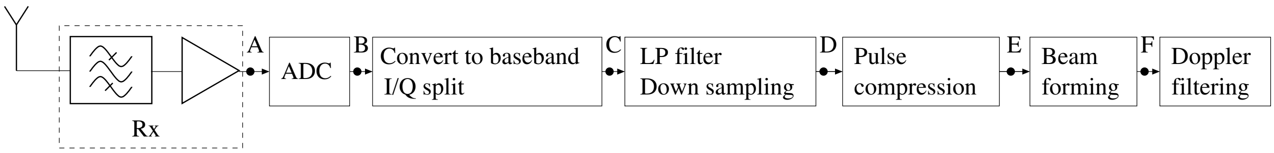

Figure 2.3: *The work flow of the signal processing from when the signal is received by the antenna to the signal processing utilised in the thesis.*

Once the signal has passed the Rx part and been amplified it is will be sampled by an ADC. The sampled signal that now is in digital form can then be subjected to digital processing. The first step in the digital processing is a conversion of the signal down to base band by shifting the centre frequency of the signal. During the same process information about the phase of the real signal is also extracted. The process of extracting phase information is traditionally performed by splitting the signal into one "real" and one "imaginary", using a phase shift. This is referred to as an I/Q split.

Having moved the signal band down to base band and extracted phase information a filter operation is performed round the base band to suppress signals outside the band of interest. This is followed by a further down sampling of the signal to what is referred to as range bin rate, which is the final sampling frequency of the signal. The theory concerning these steps are explained in section 2.5. Next a correlation between the input signal and the outgoing pulse, which is known, is performed to increase the range accuracy of the target. In radar language this is known as pulse compression, given that the width of the pulse is compressed to a maximum peak. Following this step the information from different receiver channels is used to determine the angular position of the target, referred to as beam forming and is explained in section 2.6.1. Lastly having used pulse compression to ascertain the radial distance of the target and beam forming to ascertain the angular position of the target, a pulse series is utilised towards the target in order to determine its radial velocity by means of doppler filtering, explained in section 2.7.

2.2 Electromagnetic wave propagation

In this section theory used to model the wave propagation and interaction outside of the electronics is treated. Initially it will describe how to classify the detectability of a target, through the means of radar cross section. Afterwards the treatment of changes to the power of the wave as it propagates is treated followed by an explanation of the change of phase of the signal due to doppler shift.

2.2.1 Radar cross section

Radar cross section (RCS) is a measurement of detectability of a target used when working with radar system. Having the units of area [m^2], the RCS is used to specify how much of an incident wave that is scattered back from the target after impact.

The formal definition of the RCS, is:[17]

$$\sigma = \lim_{R\to\infty} 4\pi R^2 \frac{|E_s|^2}{|E_0|^2} \tag{2.1}$$

where E_s is the electric field strength measured at the radar after scattering at the target, E_0 is the electric field strength of the incident wave to the target at target distance R from the antenna.

2.2.2 Radar equation

In order to simplify calculations we initially start with the assumption that our antenna is an isotropic radiation point source with an output power P_t. Given that the power is radiated isotropically the power at a target object, P_o, at distance R from the antenna is equal to the ratio of the spherical shell with radius R and the RCS, σ, of the object.

$$P_o = P_t \frac{\sigma}{4\pi R^2} \tag{2.2}$$

Here we have made the assumption that the object is treated like a thin sheet with an effective area, σ, that takes into account geometrical deviations and scattering direction of the object and simplifies it into a thin sheet absorbing all the power corresponding to its area.

The object then re-emits the power, acting like a point source, resulting in a received power at the receiver according to (2.3).

$$P_r = P_o \frac{A_{eff}}{4\pi R^2} \tag{2.3}$$

where A_{eff} is the effective aperture of the receiver antenna, which can be expressed using the receiver gain, G_r, wavelength of the received wave, λ, as[17]

$$A_{eff} = \frac{G_r \lambda^2}{4\pi} \tag{2.4}$$

Combining equations (2.2), (2.3), (2.4) and incorporate the transmission gain, G_t, to the transmitted power in order to compensate for the assumption of isotropic radiation source we then end up in the ideal radar equation[17]

$$P_r = \frac{P_t G_t G_r \lambda^2 \sigma}{(4\pi)^3 R^4} \tag{2.5}$$

2.2.3 Doppler shift

A doppler shift means that the observed frequency is different in different inertial frames connected by a Galilean coordinate transformation[9]. In order to explain it take a plane wave. The phase, ϕ of a plane wave is an invariant quantity and must therefore be the same in inertial frame K and K'. Describing the phase using angular frequency, ω, in these two inertial frame connected by a Galilean coordinate transformation results in (2.6)

$$\phi = \omega \left(t - \frac{\vec{n} \cdot \vec{x}}{c} \right) = \omega' \left(t' - \frac{\vec{n}' \cdot \vec{x}'}{c'} \right) \tag{2.6}$$

where $\vec{n}$ is the unit wave normal and c the speed of light. Obeying Galilean relativity the coordinate $\vec{x}'$ and time t' in frame K' can be expressed as

$$\vec{x}' = \vec{x} - \vec{v}t$$
$$t' = t$$

Combining (2.6) & (2.7) we can express K in terms of K'

$$\omega \left[t' \left(1 - \frac{\vec{n} \cdot \vec{v}}{c} \right) - \frac{\vec{n} \cdot \vec{x}'}{c} \right] = \omega' \left(t' - \frac{\vec{n}' \cdot \vec{x}'}{c'} \right) \tag{2.7}$$

Since (2.7) must hold for all t' and $\vec{x}'$ their coefficients must be equal and we get

$$\begin{cases} \vec{n} = \vec{n}' \\ \omega' = \omega \left(1 - \dfrac{\vec{n} \cdot \vec{v}}{c} \right) \\ c' = c - \vec{n} \cdot \vec{v} \end{cases} \tag{2.8}$$

The effect of (2.8) from radar perspective is that should we send a wave in direction $\vec{n}$ towards a target with relative velocity $\vec{v}$ the radial part of the velocity of the target will introduce a phase shift according to (2.8). Since in the radar case when transmitter and receiver is at the same point in space time we will experience twice the phase shift according to:

$$\Delta f = f - f_0 = -2 f_0 \frac{v_r}{c} \tag{2.9}$$

where f_0 is the transmitted frequency and v_r is the relative radial velocity between radar and target.

2.3 Electronic simulation

This section will present the theory used for simulating the electronics in the Rx block presented in figure 2.3, to be more precise, the theory used to simulated the non linear amplifiers and noise in the receiver will be presented, beginning with a section containing parameter definitions used in the amplifier model. In order to simulate the electronic circuits of the radar system we use the software Visual System Simulator$^{\mathrm{TM}}$ (VSS) from national instruments[21]. VSS is a complete software suite to simulate communication systems and is the platform used for the circuit design and simulations in this thesis.

2.3.1 Parameter definitions

For clarity we here introduce some parameters used to classify electronic components. This so that the following section becomes less bloated.

Amplifiers

In order to classify a amplifier there are certain parameters that often are used, these are presented in figure 2.4. We have the 1dB compression point, $\mathrm{P}_{1\mathrm{dB}}$, which is defined as the output power at which the response is compressed by 1dB from a hypothetical linear response [5] as explained in equation (2.10).

$$1\mathrm{dB} = P_{out,L}(P_{in}) - P_{out,NL}(P_{in}) = P_{1\mathrm{dB}} - P_{out,NL}(P_{in}) \tag{2.10}$$

where subscript L and NL denotes linear respectively non-linear output function.

Next we have the saturated output power $\mathrm{P}_{\mathrm{sat}}$, which is the maximum output power achievable from an amplifier[15].

$$P_{\mathrm{sat}} = \lim_{P_{in} \to max(P_{in})} P_{out,NL} \tag{2.11}$$

Moving on, the parameter IP_2 is used for the second-order compression point (or SOI), where the the linear term and the quadratic term intersect with each other.[20]. Analogous the third-order interception point (IP_3 or TOI) is the intersection between the linear and cubic term[20]. Given these points on the linear response the corresponding input and output power is denoted IIP_2 and OIP_2 and analogous for IP_3.

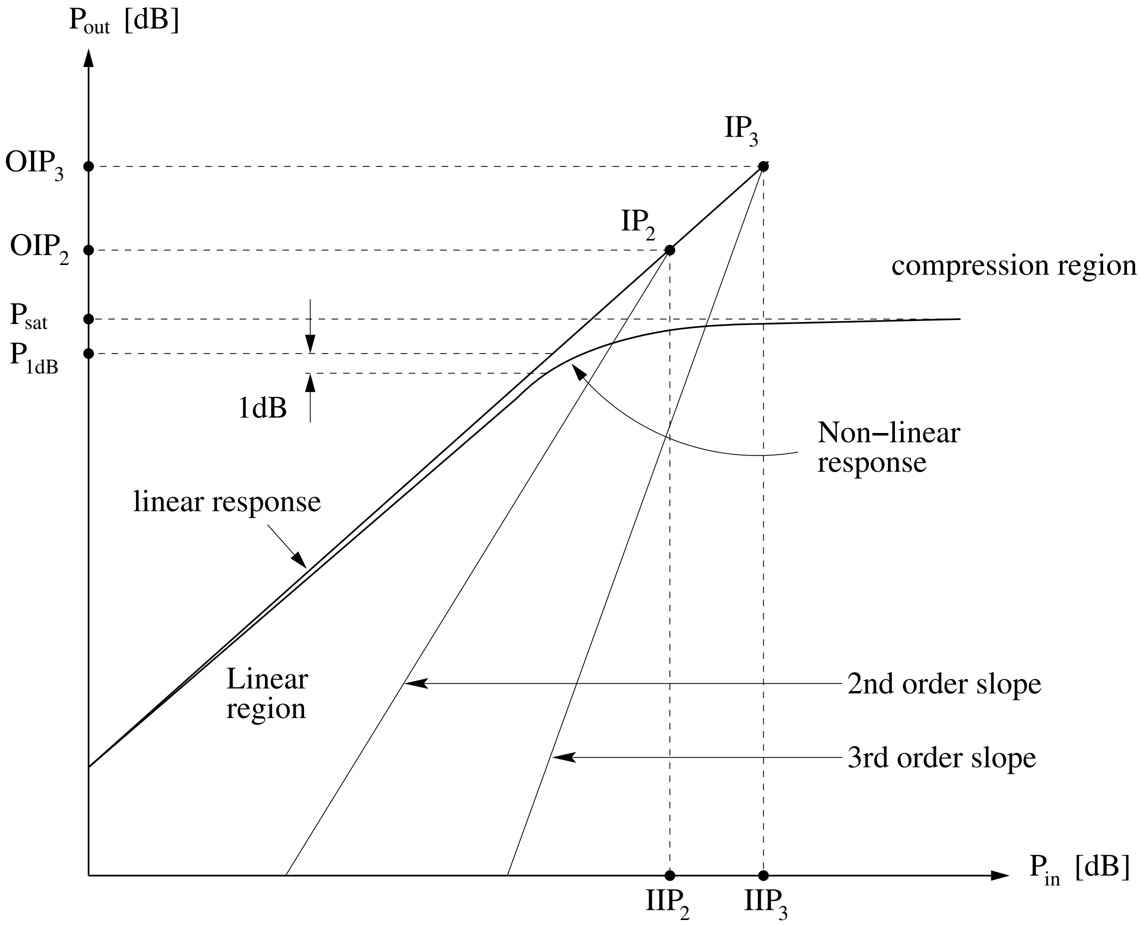

Figure 2.4: *The figure shows the output power of an amplifier as a function of input power. Detailed in the figure are the position of some parameters commonly used to describe a non-linear amplifier.*

2.3.2 Modelling of Amplifier

In order to model non linearity of amplifiers in the system VSS implements a fifth order polynomial, where the higher order terms are corrections to the ideal linear amplification designed to contribute as a decrease of amplification. The output voltage V_{out} is expressed as [2]:

$$V_{\text{out}} = g(V_{in}) = a_1 V_{\text{in}} + a_2 V_{\text{in}}^2 + a_3 V_{\text{in}}^3 + a_5 V_{\text{in}}^5 \tag{2.12}$$

Where the second and third order term generates the second and third order intermodulation and the fifth order, V_{in}^5 is used to separate the $\mathrm{P}_{1\text{dB}}$, from IP_3. The first order term V_{in} is the ideal linear gain. The coefficient a_2 and a_3 in equation (2.12) will the determined using the expansion coefficients of a 2-tone input. A table of the expansion coefficients can be found in appendix A.

Since coefficient a_1 in equation (2.12) is the linear gain it assumed positive and is expressed as

$$a_1 = 10^{\text{GAIN}/20}. \tag{2.13}$$

with GAIN being real and given in dB.

In order to determine the coefficient a_2 VSS takes a 2-tone input $V_{\text{in}} = A\cos(\omega_1 t) + B\cos(\omega_2 t)$ where the input voltage is the input voltage corresponding to IP_2, giving $V_{\text{in}} = \mathrm{vIIP}_2$. Since the second order term is designed to generate the second order intermodulation higher order terms are neglected when determining the constant a_2. By then assuming that the amplitude of the 2-tone input is equal and $A = B =$vIIP$_2$ and comparing the amplitudes of the linear first order component and the second order intermodulation product we get the relation:

$$|a_2 AB| = \left|a_2 \mathrm{vIIP}_2^2\right| = |a_1 \mathrm{vIIP}_2| \tag{2.14}$$

and the coefficient a_2 can be determined to be

$$a_2 = {}^{(+)}_{-} \frac{a_1}{\mathrm{vIIP}_2}. \tag{2.15}$$

By assuming that the second order contributes to the compression the negative value of (2.15) is used and in a similar fashion the value of coefficient a_3 is determined using the 2-tone input at IP_3 instead of IP_2. Assuming $A = B = \mathrm{vIIP}_3$, where vIIP_3 is the input voltage corresponding to IP_3 and that the higher fifth order components is small compared to the third order the comparison between the amplitude of the linear component with those of the third order intermodulation product gives

$$\left|a_3 \frac{3}{4} A^2 B\right| = \left|a_3 \frac{3}{4} A B^2\right| = \left|a_3 \frac{3}{4} \mathrm{vIIP}_3^3\right| = |a_1 \mathrm{vIIP}_3| \tag{2.16}$$

Once again assuming that the higher order contributes to the compression results by using the negative value of a_3 gives us the final expression for a_3

$$a_3 = {}^{(+)}_{-} \frac{4}{3} \frac{a_1}{\mathrm{vIIP}_3^2} \tag{2.17}$$

What now remains is to determine a_5. In contrast to a_2 and a_3, a_5 is calculated using one-tone analysis at the fundamental frequency. The expansion of equation (2.12) using $V_{\mathrm{in}} = A\cos(\omega t)$ then becomes

$$\begin{aligned} V_{\mathrm{out}} = & \left(a_1 A + \frac{12 a_3 A^3}{16} + \frac{10 a_5 A^5}{16}\right)\cos(\omega t) + \frac{8 a_2 A^2}{16}\cos(2\omega t) \\ & + \left(\frac{4 a_3 A^3}{16} + \frac{5 a_5 A^5}{16}\right)\cos(3\omega t) + \frac{a_5 A^5}{16}\cos(5\omega t) + \frac{8 a_2 A^2}{16} \end{aligned} \tag{2.18}$$

Given that only the first, third and fifth order contributes to the signal at the fundamental frequency, the power of the non-linear term is equated at $\mathrm{vIP}_{1\mathrm{dB}}$ for the fundamental frequency. Using the fact that $\mathrm{vIP}_{1\mathrm{dB}}$ lies 1dB below the linear term and comparing the amplitudes of the linear term subtracted by 1dB and the amplitude for the non linear fundamental frequency amplitude yields

$$\left|a_1 \mathrm{vIP}_{1\mathrm{dB}}\, 10^{-1/20}\right| = \left|a_1 \mathrm{vIP}_{1\mathrm{dB}} + a_3 \frac{3}{4} \mathrm{vIP}_{1\mathrm{dB}}^3 + a_5 \frac{10}{16} \mathrm{vIP}_{1\mathrm{dB}}^5\right| \tag{2.19}$$

and thus

$$a_5 = \frac{8\left(a_1 \mathrm{vIP}_{1\mathrm{dB}}(10^{-1/10} - 1) - a_3 \frac{3}{4} \mathrm{vIP}_{1\mathrm{dB}}^2\right)}{5 \mathrm{vIP}_{1\mathrm{dB}}^4} \tag{2.20}$$

When the amplifier nears compression and passes the 1dB compression point , VSS treats this by scaling the amplitude of the input voltage V_{in} prior to evaluation in the polynomial in equation (2.12). During the implementation of saturation in the amplifier VSS initially finds the first positive maximum of equation (2.12) and assigns $\mathrm{vOSat}_{\max} = V_{\mathrm{out}}$ and $\mathrm{vSSat}_{\max} = V_{\mathrm{in}}$. These values then serves as upper boundaries to the output voltage. Thereafter VSS checks this value against user defined saturation level, vOSat, and if $\mathrm{vOSat}_{\max} \geq$ vOSat then VSS calculates the output voltage from equation (2.12) and use vOSat as the upper boundary.

The actual shaping of the input signal to the amplifier is executed using a quadratic equation, $V_{\mathrm{Scale}}(V_{\mathrm{in}})$, obeying the relations[2]:

$$V_{\mathrm{Scale}}(\mathrm{vIP1dB}) = \mathrm{vIP1dB} \tag{2.21a}$$

$$\frac{\mathrm{d}V_{\mathrm{Scale}}}{\mathrm{d}V_{\mathrm{in}}}(\mathrm{vIP1dB}) = 1 \tag{2.21b}$$

$$V_{\mathrm{Scale}}(\mathrm{vISat}) = \mathrm{vSSat} \tag{2.21c}$$

$$\frac{\mathrm{d}V_{\mathrm{Scale}}}{\mathrm{d}V_{\mathrm{in}}}(\mathrm{vISat}) = 0 \tag{2.21d}$$

where vISat is the maximum input amplitude scaled by V_{Scale}. Any input amplitudes $V_{\text{in}} > \text{vISat}$ are then clipped to vSSat. The end results is the amplifier model presented in equation (2.22).

$$V_{ut} = \begin{cases} g(V_{\text{in}}) & , |V_{\text{in}}| \leq \text{vIP1dB} \\ g\left(V_{\text{Scale}}(V_{\text{in}})\right) & , \text{vIP1dB} < |V_{\text{in}}| \leq \text{vSSat}_{\text{max}} \\ \text{vOSat}_{\text{max}} & , \text{vSSat}_{\text{max}} < |V_{\text{in}}| \end{cases} \tag{2.22}$$

2.3.3 Noise

Since we have statistical fluctuation of electronics charges in all conductors, these fluctuation will create potential differences resulting in the appearance of noise in the system[10]. This type of noise, usually termed thermal noise, depends on the temperature, T, of the system, its resistance, R, so the root mean square (RMS) voltage for a circuit with constant amplification in the bandwidth $\Delta f = f_2 - f_1$ round centre frequency, f_c, can be written as [13]

$$V_{RMS}^2 = 4hf_cR\Delta f\ \overline{n}_{Pl} \tag{2.23}$$

where k_B is the Boltzmann constant and $\overline{n}_{Pl}$ is the Planck distribution[16]

$$\overline{n}_{Pl} = \frac{1}{e^{(hf_c)/(k_BT)} - 1} \tag{2.24}$$

When working with microwave frequencies we have that $hf_c << k_BT$ and we can expand (2.24) using Taylor expansion as

$$\overline{n}_{Pl} \approx \frac{1}{\left(1 + \frac{hf_c}{k_BT} + \mathcal{O}\left(\left(\frac{hf_c}{k_BT}\right)^2\right)\right) - 1} \approx \frac{k_BT}{hf_c} \tag{2.25}$$

and therefore the equation (2.23) can be expressed as the Rayleigh–Jeans approximation

$$V_{RMS} = \sqrt{4k_BTR\Delta f} \tag{2.26}$$

Now given that we have an electric circuit and we use Jacobi's law which states that maximum power transfer occurs when the load resistance equals that of the source. Since systems are designed for maximum power transfer this also applies for the noise and we can write the transferred noise power to a perfect load as [13]

$$P = \left(\frac{V_{RMS}}{2R}\right)^2 R = \frac{V_{RMS}^2}{4R} = k_BT\Delta f \tag{2.27}$$

When working with signals it is common to work with signal to noise ration (SNR). The SNR is as the name applies the ratio between the power of a signal, P_{signal} to that of the noise power, P_{noise}

$$SNR = \frac{P_{signal}}{P_{noise}} \tag{2.28}$$

this is also used to characterise components by means of the noise factor, F:

$$F = \frac{SNR_{in}}{SNR_{out}} \tag{2.29}$$

which specifies the SNR ratio between input and output. Both SNR and noise factor also has an equivalent decibel form labelled as SNR_{dB} and noise figure, NF respectively.

When simulating noise in VSS the noise is modelled as white Gaussian noise with power according to[2]

$$P_{noise} = (F - 1)k_BTf_s \tag{2.30}$$

which is equation (2.27) with the addition of the term $(F - 1)$ to account for the noise figure of the amplifier and the bandwidth, Δf is replaced with the sampling frequency f_s.

2.4 Filters

During the transmission and receiving of radar signals the outgoing wave is typically filtered in order to remove unwanted interference from frequency regions other then the bandwidth we transmit at. Simulation-wise we see the radar pulse (or consecutive radar pulses) as a finite sequence x_n in time-domain, where x_n corresponds to the voltage values in the electric circuit. Applying a filter to the sequence x_n is easily done by multiplying the desired filter, h_n, with length N in the frequency domain with our sequence x_n in order to yield a filtered sequence, y_n:

$$\widetilde{y}_n = (\widetilde{h}\,\widetilde{x})_n \tag{2.31}$$

where $\sim$ denotes the discrete Fourier transform, eg. $\widetilde{\mathbf{x}} = \mathcal{F}_N\{\mathbf{x}\}$, using linear map $\mathcal{F}_N : \mathbb{C}^N \to \mathbb{C}^N$. Equation (2.31) can be expressed in time domain as a finite convolution [6]

$$y_n = (h * x)_n = \mathcal{F}_N^{-1}\left\{\widetilde{h}\,\widetilde{x}\right\}_n = \sum_{i=0}^{N-1} h_i x_{n-i} \tag{2.32}$$

2.4.1 Window function

Just as the name implies a window function, $g(x_n)$, is a function applying a window to a function, $f(x_n)$, so that the amplitude outside a given interval goes to zero. A more formal definition is that the product $x_n g(x_n)$ must be square integrable.[3]

Taylor window

In radar antenna operations it is common to utilise Taylor windows[23]. The Taylor window is designed to shift, or dilate, the zeros of the array factor so that they move the zeros closest to the main beam further away in order to achieve near constant side lobe levels.

The weights of the Taylor window for a linear array of length L is generated using equation (2.33)[11]:

$$g(x) = F(0, A, \overline{n}) + 2\sum_{m=1}^{\overline{n}-1} F(m, A, \overline{n}) \cos\left(\frac{2m\pi x}{L}\right), \quad x \in [-L/2, L/2] \tag{2.33}$$

where z_n are the zero locations of the synthesised pattern given by:

$$\begin{aligned} z_n &= \pm\sigma(A^2 + (n-1/2)^2)^{1/2} && , 1 \le n \le \overline{n} \\ &= \pm n && , \overline{n} \le n \le \infty \end{aligned} \tag{2.34}$$

Here σ is the dilution factor that dilates the ideal array factor so that its closest zeros moves away from the main beam. It's expressed according to equation (2.35) as

$$\sigma = \frac{\overline{n}}{\left[A^2 + (n\overline{n} - 1/2)^2\right]^{1/2}} \tag{2.35}$$

where $\overline{n} \in \mathbb{Z}$ is integers corresponding to zero locations, z_n, and the coefficients $F(z, A, \overline{n})$ are evaluated according:

$$F(m, A, \overline{n}) = \frac{[(\overline{n}-1)!]^2}{(\overline{n}-1+m)!(\overline{n}-1-m)!} \prod_{n=1}^{\overline{n}-1}\left[1 - \frac{m^2}{z_n^2}\right] \tag{2.36}$$

and A is defined as:

$$A = \frac{\operatorname{arccosh}(r)}{\pi} \tag{2.37}$$

where r is the side lobe ratio.

The resulting window and frequency response given by creating a window for a 13 element array with $\overline{n} = 4$, and a desired side lobe difference of -30dB is presented in figure 2.5.

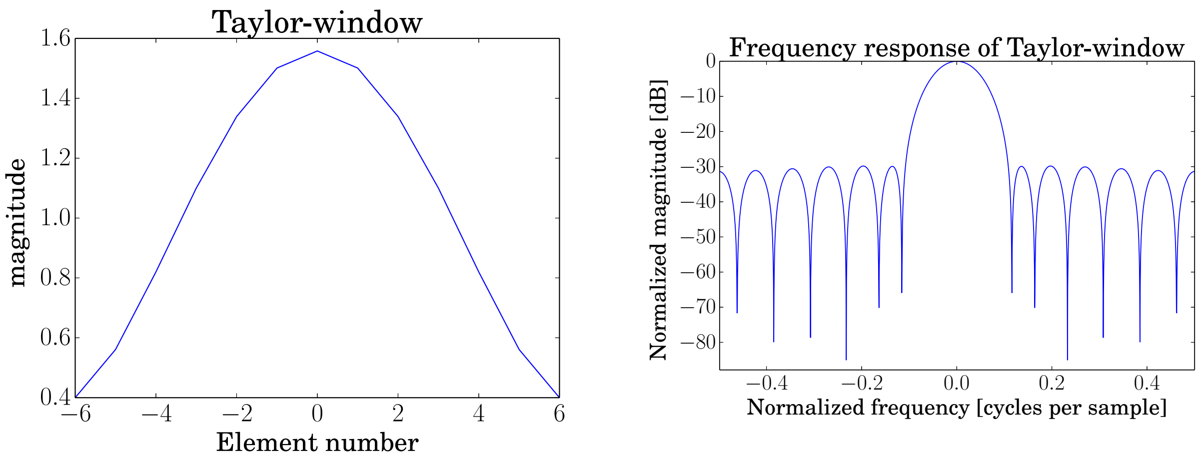

Figure 2.5: *The figures shows the Taylor window generated from equations* (2.33)-(2.37) *and its frequency response when generated for a 13 element array with* $\overline{n} = 4$, *and a desired side lobe difference of -30dB.*

Blackman-Harris

The Blackman-Harris window is a window where the width of the main-lobe has been traded for a better side-lobe suppression, the window of length N is expressed as[7]:

$$w(n) = a_0 - a_1 \cos\left(\frac{2\pi}{N}n\right) + a_2 \cos\left(\frac{2\pi}{N}2n\right) - a_3 \cos\left(\frac{2\pi}{N}3n\right) \;, n = 0, 1, 2, ...N - 1 \qquad (2.38)$$

using the coefficients in table 2.1

Table 2.1: The table shows the coefficients for the Blackman-Harris window in equation (2.38).

a_0	a_1	a_2	a_3
0.35875	0.448829	0.14128	0.01168

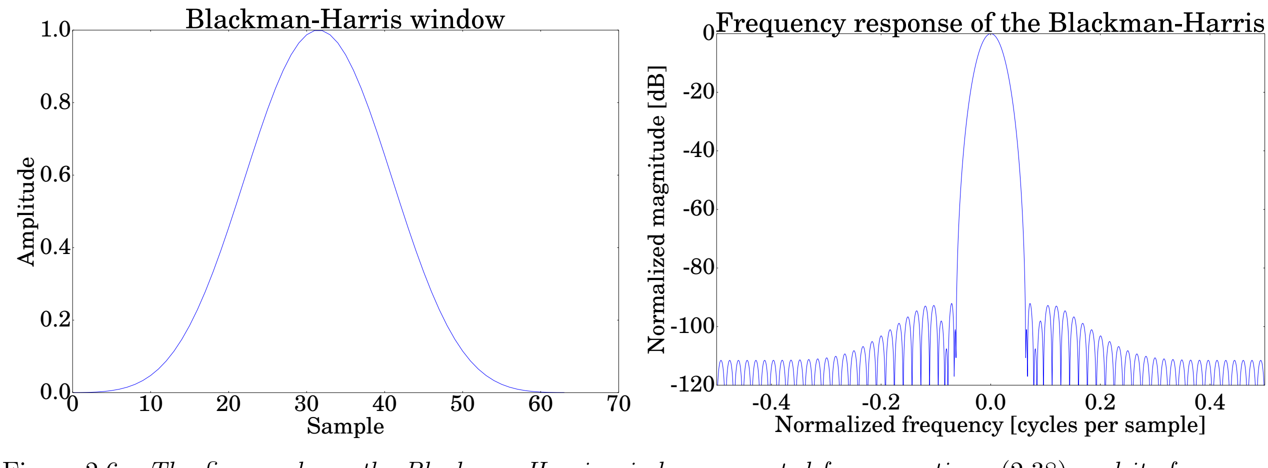

Figure 2.6: *The figures shows the Blackman-Harris window generated from equations* (2.38) *and its frequency response when generated for 64 samples.*

2.5 Sampling of signals

In the physical application the real world will take care of the electronic simulation and will forward its output to our ADC. Here the ADC will sample the signal using a sampling frequency f_s. The nature of how an ADC samples the signal differs from model to model. Common to them all however is that they have an quantisation level that defines the accuracy of the sampling, that is a signal is given a value s if it is in the region $s \pm \frac{LSB}{2}$, where LSB is the Least Significant Bit defined as [14]

$$LSB = \frac{V_{FSR}}{2^n} \tag{2.39}$$

for binary converters. Here $V_{FSR} \in [V_-, V_+]$ is the full scale range of input voltage and n is the number of bits. For our purpose it is sufficient to know which voltage levels the ADC can detect and in which voltage range, the rest is a rounding operation.

Once sampled the signal is then in a band, centred round a centre frequency, f_0. In order to decrease the computational work it is customary to down-mix this signal to base band, effectively moving the centre frequency to 0Hz. Since the sampled signal is real, you also want to extract phase information by performing an I/Q separation[23], where I is the in-phase component and Q is the quadrature-phase component separated from each other with a $\pi/2$-phase shift. Traditionally with "analogue" radar these steps are performed in hardware. With digital radar however this operation is performed digitally and can be combined with the down mixing to base band resulting in that we can write the the complex base band signal, $r_{base}[m]$, using our real sampled signal, $r_{in}[m]$, as:

$$r_{base}[m] = e^{-2\pi i (f_0/f_{s,rx})m} r_{in}[m] \tag{2.40}$$

Next you want to filter the base band signal to remove noise and higher order harmonics using a low pass filter in order to suppress regions outside the signal bandwidth. This can be can be done together with down sampling to the signal band by performing a decimation. By using a low pass filter, $h[n]$, with length K, and sample every N_s output, the final output can be written as:

$$r_{out}[n] = \sum_{m=0}^{K-1} h[N_s n - m] r_{base}[m] \tag{2.41}$$

with the final range bin rate as f_s/N_s.

2.5.1 Folding of harmonics during ADC sampling

Since the digital radar system also amplifies signals outside the signal band and that these in turn might give rise to higher order harmonics it is of interest to ascertain where different frequencies will fold when the RF-signal is being undersampled. A representation of the different folding placements from different frequencies and their harmonics when sampled with a sampling frequency of 960MHz are presented in figure 2.7. Also presented in the figure is the band that finally is extracted after the decimation presented in equation (2.41) for a signal with centre frequency of 1.3GHz.

By observing this figure it can be seen that some frequencies, like 1280MHz, have positions where the different harmonics fold into the same frequency region. The centre frequency at 1.3GHz however is chosen so to avoid the overlap from the folding of the harmonics in the final sampling band.

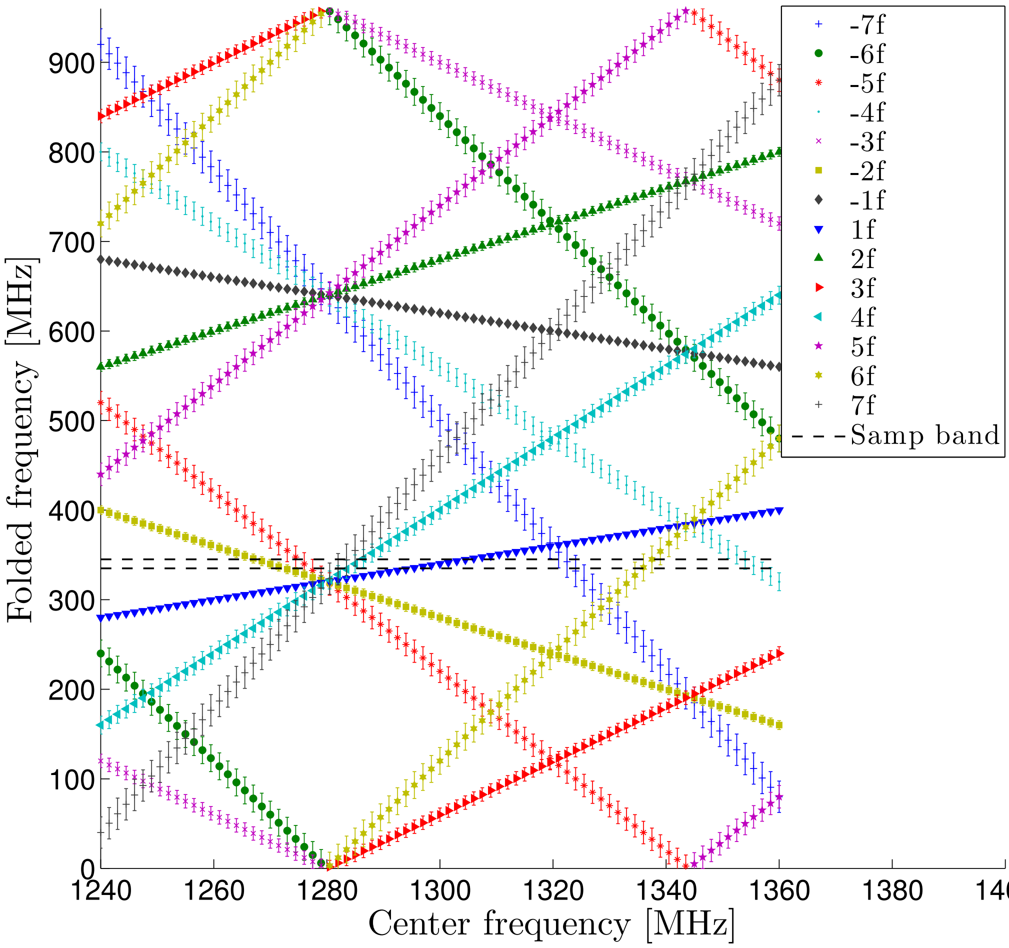

Figure 2.7: *The figure shows the frequency placement of a 5 MHz bandwidth centred round different frequencies and several harmonics as they are under sampled with a sampling frequency of 960MHz. The bars represents the width of the 5MHz band.*

2.5.2 Signal clipping

Should a signal be strong enough to exceed the voltage intervals of the ADC the signal will be clipped. This process basically turn the signal towards a square wave with the signal getting closer to the ideal square wave the higher above the ADC interval it gets. Given this relation the harmonics generated from the clipping is that of the square wave and the amplitudes are bounded from above by those of the square wave, $f(\theta)$, (2.42)[6]

$$f(\theta) = \frac{4}{\pi} \sum_{n=1}^{\infty} \frac{\sin((2n-1)\theta)}{2n-1} \tag{2.42}$$

scaled to the proper amplitude. This also means that only odd harmonics of the clipped signal will be generated

2.6 Antenna array

In this section, theory for performing the beam forming using the channel data from a ULA will be presented. After the theory of beam forming has been presented the concept of tapering to decrease side lobes will be presented using theory from section 2.4.1.

2.6.1 Beam forming

One of the advantages of having an antenna array is the fact that it lessens the need of mechanical steering. Instead you can "create" you own beam steering by shifting the phase of the Rx/Tx elements. If you look at figure 2.8, where we have a case of a multiple antennas idealised as dot and a plane wave relative their position.

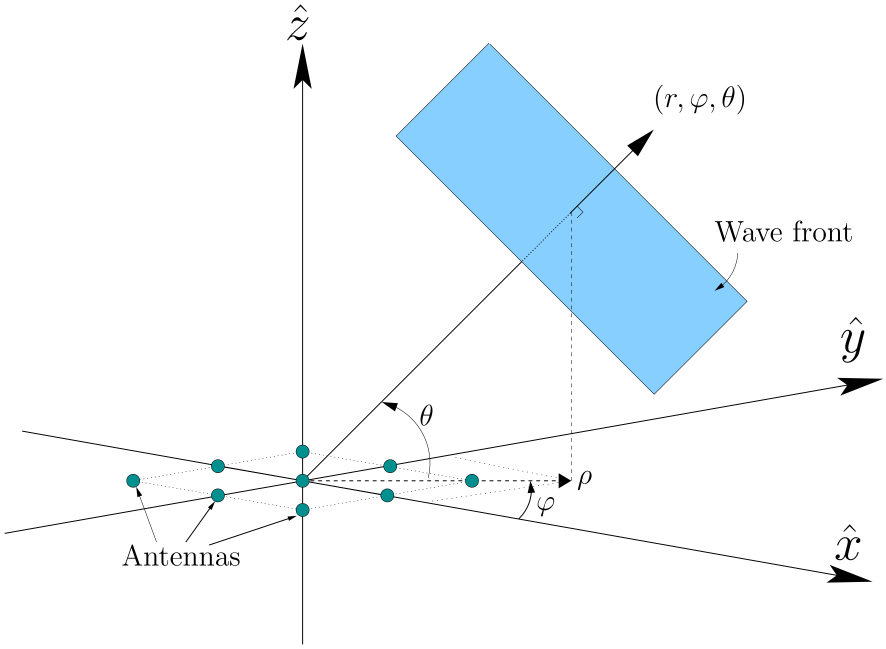

Figure 2.8: *The figure states the inertial system chosen for the antenna arrays ($\hat{x}, \hat{y}, \hat{z}$) and a representation of a plane wave relative the antenna coordinates.*

It is clear from the figure 2.8 that should this be an incident wave with in radial direction $\vec{r} = (r, \varphi, \theta)$ each antenna with coordinate position $\vec{x}_i$ would experience interaction with a time delay δt_i relative origo. By defining that we measure time and distance from origo in our initial system we can let the wave propagate until it reaches origo. In this position we can calculate the delay by taking the projection of the antenna coordinates onto the direction of the incident wave.

$$\delta t_i(\vec{r}) = \frac{\vec{r}}{||\vec{r}||} \cdot \vec{x}_i \frac{1}{c} \tag{2.43}$$

where c is the speed of light in the media. By knowing the frequency of the wave, f, we can we can calculate the needed phase shift, $\phi = 2\pi f \delta t_i$ and the final change needed to be made to an measured voltage, $V(t)$ becomes

$$V_{i,\text{shifted}}(t) = V_i(t) e^{i\phi_i} \tag{2.44}$$

The same reasoning can be applied for transmission of the radar pulse, where you shift the signal for each antenna element so that the transmitted wave aligns in a desired $\vec{r}$ direction. In order to finally get the beam summation in each direction we simply sum over all the the shifted voltages

$$V_{sum}(\vec{r}, t) = \sum_i V_i(t) e^{i\phi_i} \tag{2.45}$$

2.6.2 Taper

Since by its nature, an antenna array is hard to shield in periphery directions, as it would counteract the advantages of the beam forming discussed in section 2.6.1. This has the effect that the radar always listens in all directions. Given the positions of the antennas we will experience less amplification in directions separate from the main lobe (bore sight), commonly referred to as side lobes.[23]

This is easily demonstrated by example, assume that we have N antennas equidistantly positioned along a straight line. We then use equation (2.45), choosing coordinate system so we only have one free variable φ and letting the signal, V_i, we shift be identically one. Then we perform the summation and get the so called array factor[23], shown in figure 2.9 for the case of a 13 element array.

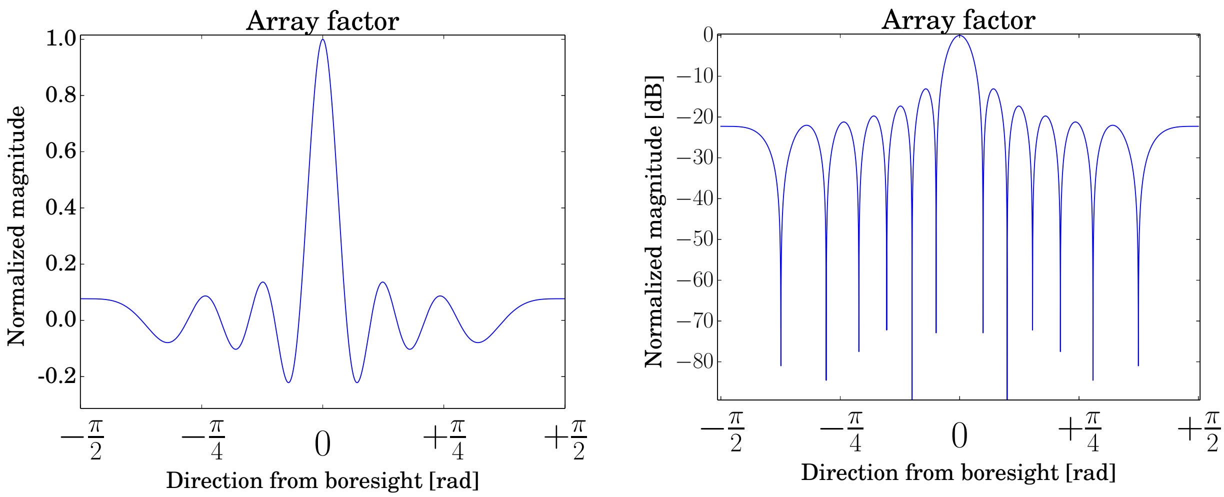

Figure 2.9: *The figures shows the array factor for a equidistantly linear 13 element array with element separation, $d = \lambda/2$.*

These side lobes constitute a problem since should we experience disturbance in some form in one of these directions it could result in a lower sensitivity or in a false detection where we think we have a target in the main beam but it is in fact just disturbance in the side lobe. There are different ways to counter this effect, by altering the way we form the main beam. One of these are tapering where we scale the contribution of different antenna elements using a window function. [23] Figure 2.10 shows the change from applying a Taylor window, detailed in section 2.4.1, to the array factor displayed in figure 2.9.

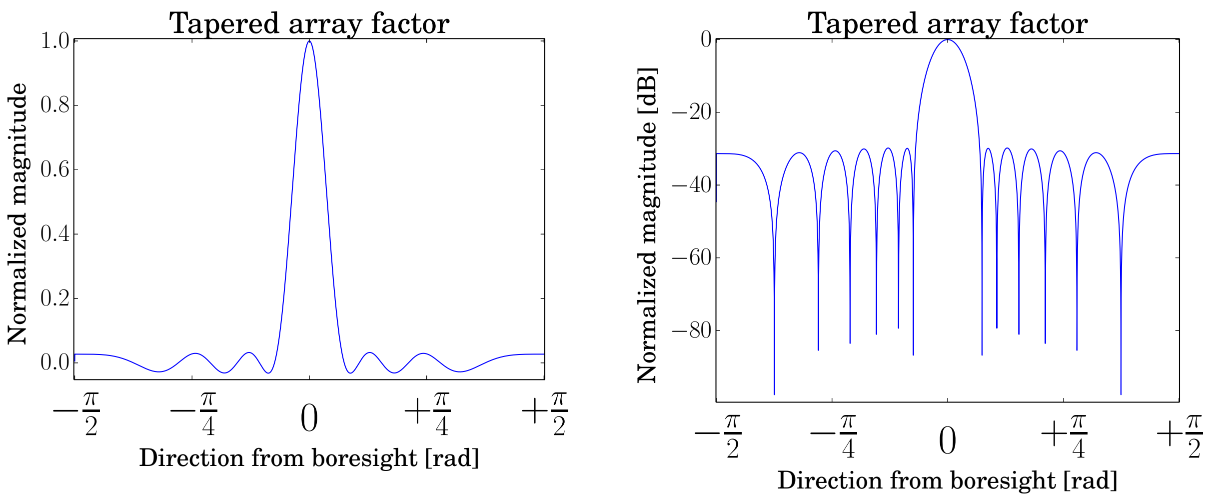

Figure 2.10: *The figures shows the array factor for a equidistantly linear 13 element array with element separation, $d = \lambda/2$, tapered with a Taylor window with -30dB side lobe levels.*

2.7 Doppler filtering

Given that an object moves when being subjected to an incident wave the reflected wave will experience a doppler shift as detailed in section 2.2.3. By observing the change in frequency from the transmitted wave due to the doppler shift, the information can be utilised to determine the targets radial velocity. In order to achieve this the target must be illuminated with a series of pulses. Should the target move each value at a fixed range value will shift during the cause of the total pulse series. By determining the periodicity of this change by means of a Fourier spectrum the doppler shift can be extracted. [23] In radar terminology this is known as creating a doppler filter bank, where each doppler filter corresponds to a Fourier coefficient. Given a PRF with frequency, f_{prf} and a doppler filter bank, consisting of N filters, the separation, Δf, of each doppler filter or position in the Fourier spectra becomes

$$\Delta f = \frac{f_{prf}}{N} \tag{2.46}$$

Combining equation (2.9) and (2.46) we can then calculate the radial velocity resolution, Δv_r, of the target for each doppler channel as.

$$\Delta f = \frac{f_{prf}}{N} = -2f_0\frac{\Delta v_r}{c} \Rightarrow \Delta v_r = -\frac{f_{prf}}{N}\frac{c}{2f_0} \tag{2.47}$$

3 Method

In this chapter the structure of the computation module is presented together with its implementations. This starts in section 3.1 with a presentation of the program structure and following this section each individual implementation of the program structure is treated in separate subsections, following the execution flow of the program.

3.1 Program structure

The goal is to create a model of the radar system that can generate input data depending on what kind of targets or signals that is of interest. The model will then perform signal processing on the output in order to determine the attributes of the target and increase the SNR of the received target echo.

For the simulation of the radar system we simulate the bulk of the program using MATLAB[19] and we are using VSS[21] for the electronic circuit simulations as detailed in figure 3.1.

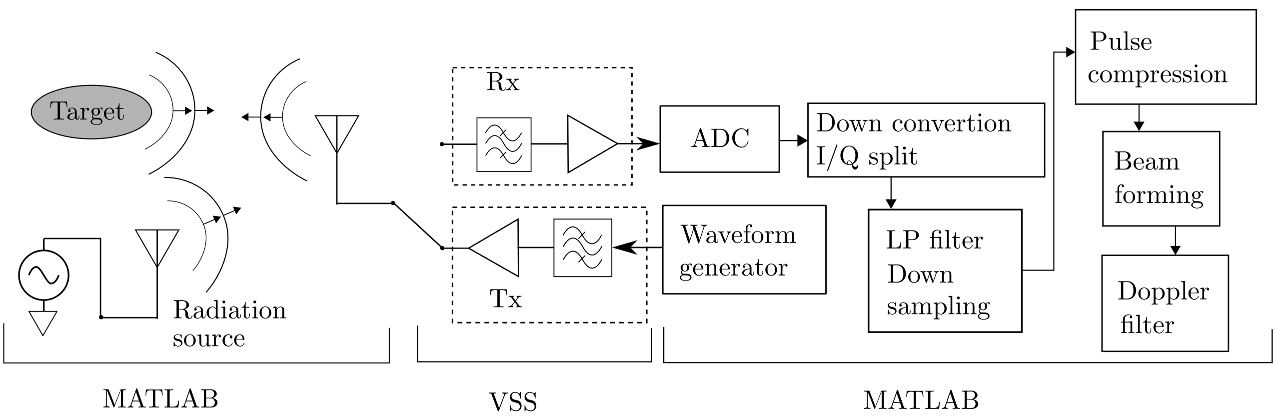

Figure 3.1: *The figure presents the distribution of simulation for different parts of the radar chain.*

The total simulation program is designed as a series of different modules, presented in figure 3.2.

Each module in figure 3.2 is then simulating a certain part in the radar chain forming a pipeline, presented in figure 3.3.

The modules takes the input in the form of a MAT-file (version 7.3)[12] which saves the data using hierarchical data format 5 (HDF5)[8], and allows partial loading of stored variables, which in turn facilitates

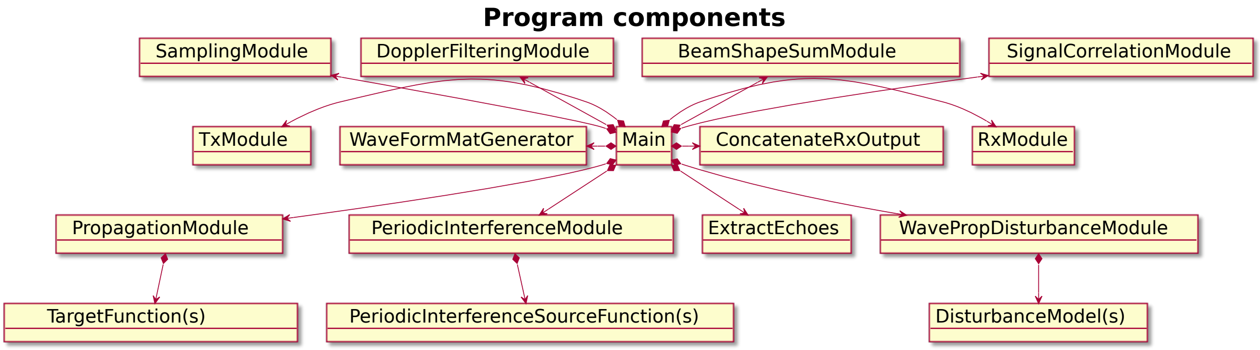

Figure 3.2: *The figure shows the composition of the main program.*

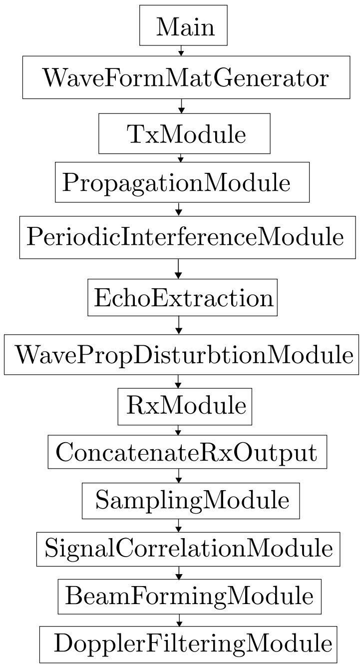

Figure 3.3: *The figure presents a flow chart of the simulation of the radar chain.*

RAM usage. The module process the data and return the results in a new file. This approach makes it easy to modify, swap, add or remove modules in the radar simulation without much re-coding as well as making it easy to analyse each step of the process.

The down side of this approach is that it requires more memory writes, which negatively effects the simulation time. The choice to use VSS to simulate the electronics instead of modelling the circuitry anew using another programming language, comes from the fact that it should be easy to test circuits already designed in said software without having to rewrite it as code.

The goal of the simulation is that given an input waveform to the Tx module and any number of target or interference models, generate a matrix containing incoming wave data into each Rx channel, perform the electronic simulations on said wave data, sample it and perform signal processing, finally yielding 3D-matrices containing data of range, direction and doppler channels. The process of data treatment is visualised in figure 3.4 & 3.5. Figure 3.4 presents the data treatment of the of the two left sections in figure 3.1 simulated using MATLAB and VSS. First it illustrate the generation of the outgoing pulse to be transmitted, explained in section 3.1.1 and 3.1.2, then send multiple pulses towards a target and collecting the returning echoes, treated in accordance with the method described in section 3.1.3 and 3.1.4. Thereafter the figure shows the preparation of the data matrix before electronic simulation, which is explained in section 3.1.5. Once prepared the data will undergo electronic simulation according to the method of section 3.1.7. The data is then treated as detailed in section 3.1.8 to produce the a matrix containing the voltage values for specific times that enters the ADC.

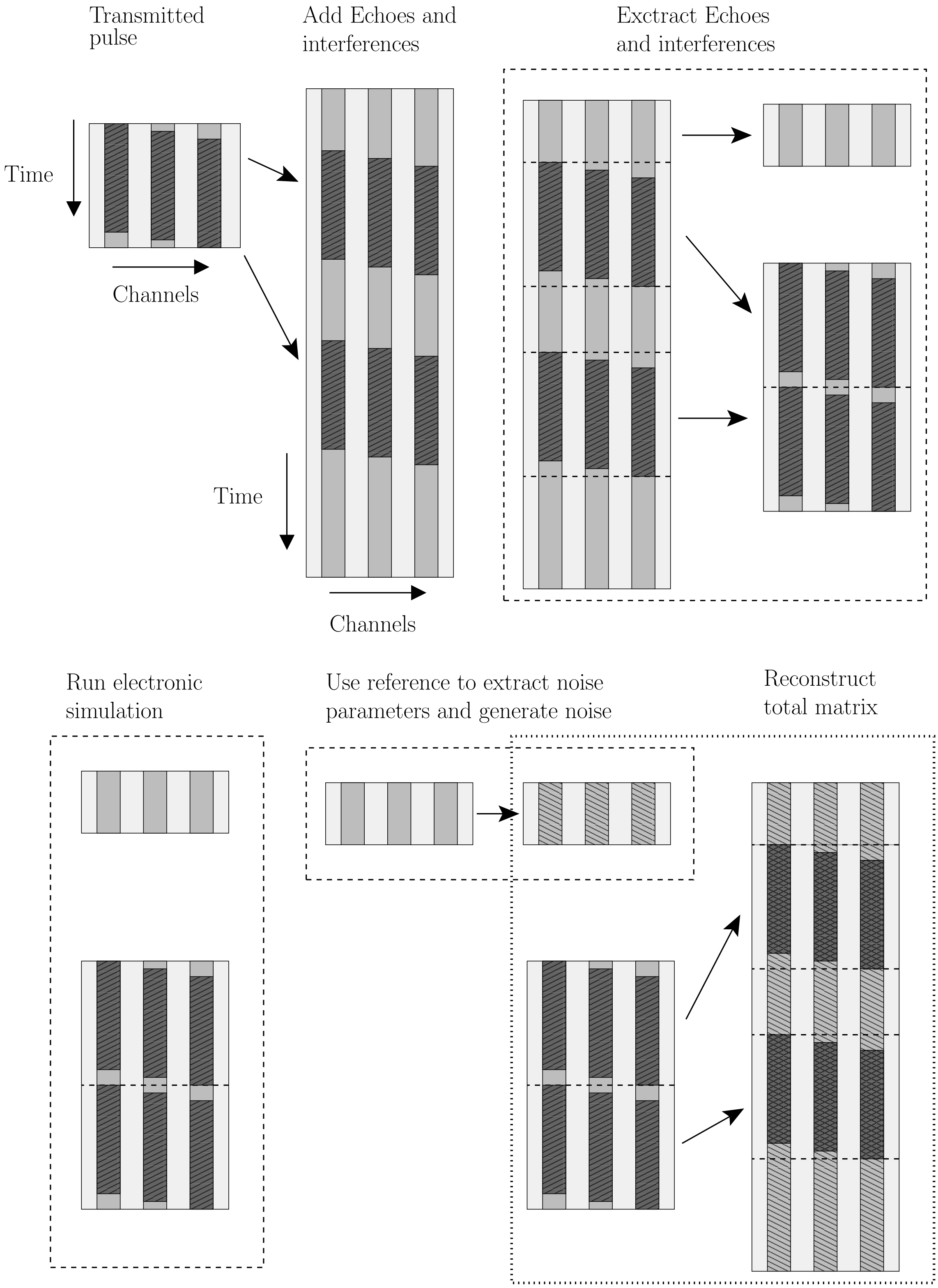

Figure 3.4: *The figures shows schematically how data is handled during simulation before signal processing. First a transmission pulse is generated. This is then used for the following pulses and, depending on the interaction with the target, the generated echoes are inserted into corresponding positions in the full time matrix. Thereafter the parts of the full matrix containing echo data are extracted into a separate matrix in order to speed up calculation time. At the same time an echo free sample is taken as a reference in order to generate noise for the final matrix containing electronic simulation output. Once the extracted matrix containing echoes has been simulated with respect to the electronics it is again split up and each pulse echo is returned to it true time position.*

Using the matrix generated, the data then undergoes the digital signal processing steps shown in figure 3.1. The data treatment of these steps are shown in figure 3.5 and the different steps are explained in sections 3.1.9-3.1.12.

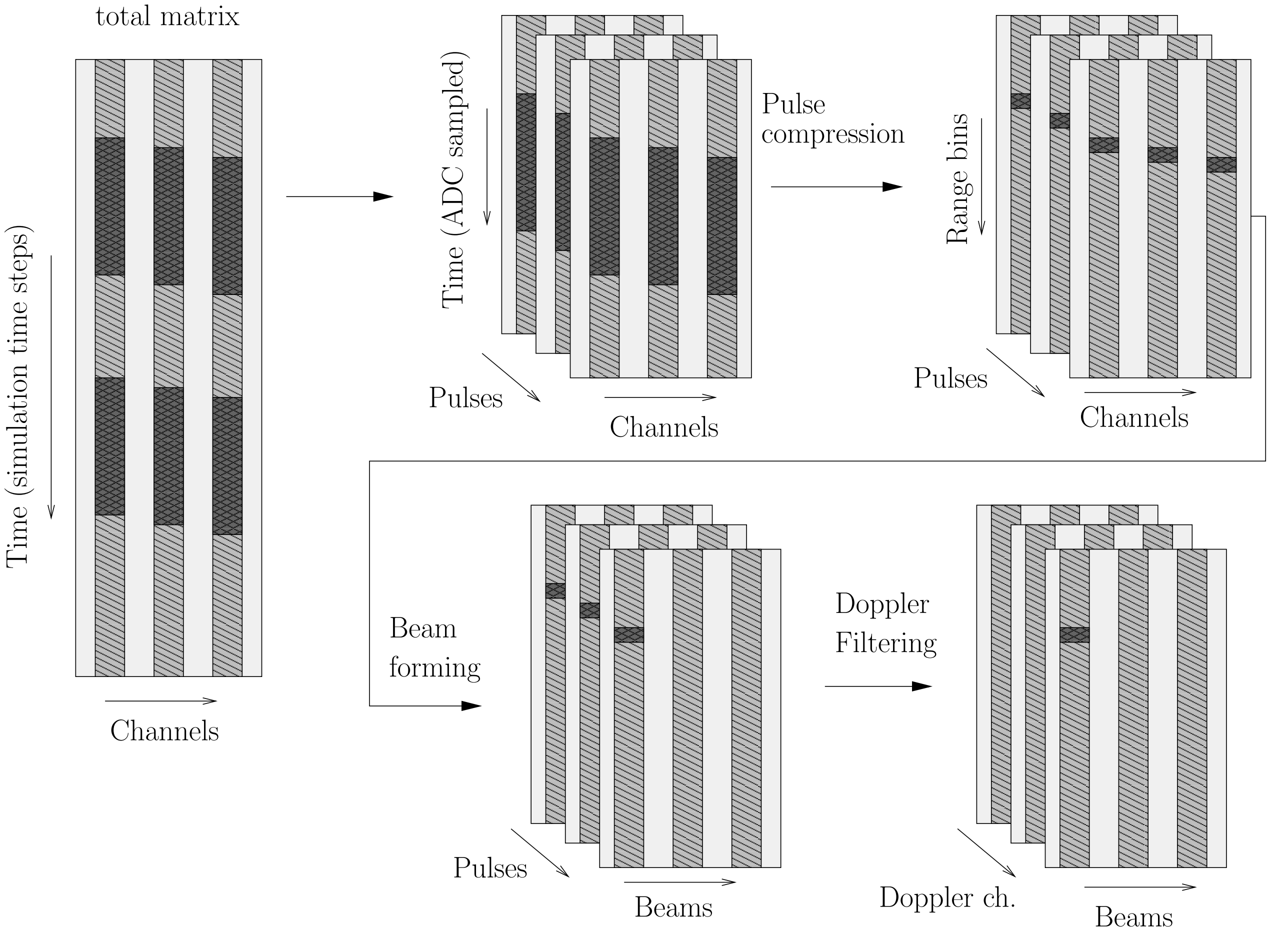

Figure 3.5: *The figure shows how the total 2D data matrix from the electronic simulation is treated during signal processing of the last 4 modules, presented in figure 3.3, to create the final 3D-matrix. First a 2D matrix is formed by calculating the position for echos and external signal in time and superposition them into the first matrix. This matrix is then sampled, greatly decreasing number of elements, and separated into pulses, forming a 3D matrix. Thereafter the matrix undergoes pulse compression, beam forming and doppler filtering and through this increase the SNR of the desired signal and concentrate its position in the 3D matrix.*

3.1.1 WaveFormMatGenerator

This module serve the purpose of providing the wave form that is to be transmitted from the radar. During the simulations performed in this thesis this has been a linear chirp (3.1)

$$y(t_n) = Ae^{i\phi_0 + 2\pi i \left(f_0 t_n + \frac{k t_n^2}{2} \right)} \tag{3.1}$$

where the coefficients has been adjusted to create at chirp with a band of 5MHz, centred round 1.3GHz.

3.1.2 TxModule

The TxModule is designed to simulated the Tx block in figure 3.1, which illustrates the electronic treatment of the transmission of the radar. The purpose of this system component is to amplify the signal it is feeded with. During this thesis the transmitter will operate linearly, as a set of amplifiers and filters, in order to focus on the effect of non-linearities generated in the receiver. Thus the Tx circuit doesn't contribute to any non-linearities.

The simulations of the electronic components was performed in VSS while being controlled through MATLAB. The communications between VSS and MATLAB is designed so that we use MATLAB to generate a Windows Powershell script (.PS1)[22] designed to control VSS using VSS' own api[1] via Component Object Model (COM)[4] . After the powershell script has been generated MATLAB executes the script letting powershell act like a COM server for the VSS COM client while simulations are running. MATLAB then waits for the electronic circuit simulation to complete, after which the simulation data is ported to the next module. A scaled down sequence diagram for this operation for the Tx module is presented in figure 3.6.

The concept is that the VSS module consists of one "dock" where the designed circuit is located. This dock is then coupled to matlab functions, which have the function to load the channel data for the incoming signal, respectively save the circuit simulated data to given matfile. This approach makes is easy to interchange circuit diagrams by changing the link to the dock, thus facilitating the system design and lowering workload.

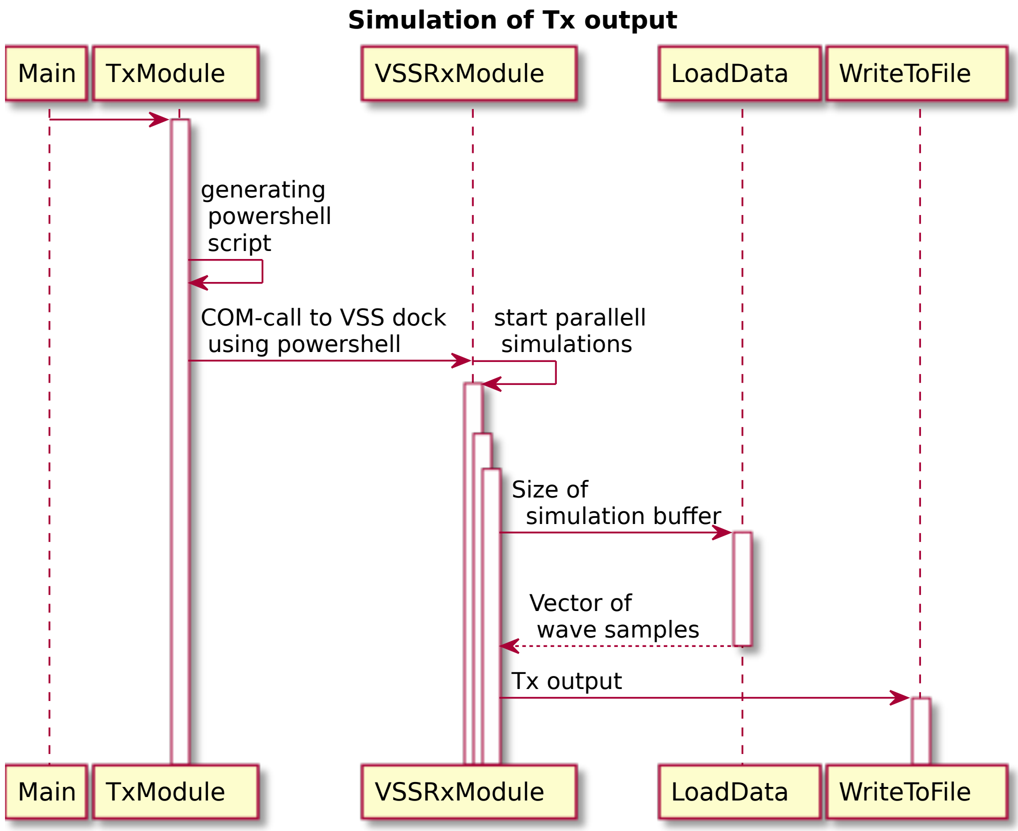

Figure 3.6: *The figures shows the sequence diagram of the Tx simulation in the TxModule. The functions LoadData and WriteToFile are both* MATLAB*-functions used for reading and writing to files.*

3.1.3 PropagationModule

This subsection treats the simulation of the propagation and target interaction of the waveform amplified with the Tx circuit according to subsection 3.1.2. The purpose being to simulate the propagation of the radar pulse to the target and back again. The module then repeats this procedure for a given number of consecutive pulses and generates a large matrix containing the resulting incoming signal to each channel of the receiver.

The target model used in this thesis is chosen to incorporate the theory of section 2.2.2 and 2.2.3. It is chosen so that given a point in time, and the present order the target was illuminated by a radar pulse, the target model will return the target's position, velocity and RCS. Then given a PRF of the radar system and the number of pulses the radar should emit during the simulation the module will treat the system as displayed in figure 3.7.

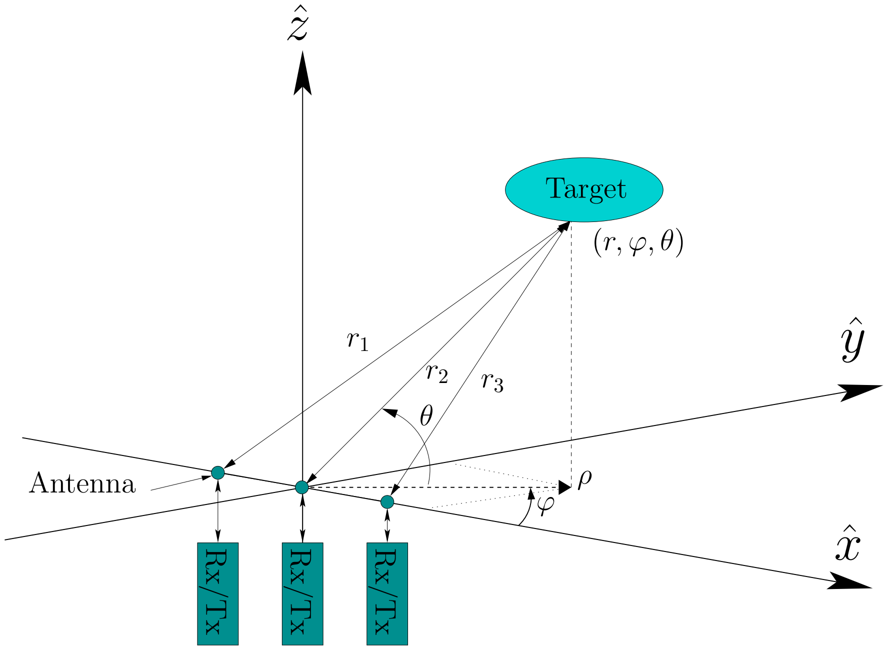

Figure 3.7: *The figure shows the inertial coordinate system for the simulations together with positions for antennas and a target. The azimuth angle, φ, is taken to be the angle in the XY-plane*

At the time of the transmission of a radar pulse the time frame is frozen. In this situation the module calculates every distance r_i between antenna position x_i and the point target using the target coordinates from the target model to express r_i as the norm

$$r_i = ||\vec{r}_{target} - \vec{x}_i|| \tag{3.2}$$

where $\vec{r}_{target}$ is the vector from origo to the target. Next it determines the amplitude of the contribution from transmission antenna i to receiving antenna j by calculating the surface power density at the target using distance r_i and then back to receiving antenna j using distance r_j. By using the relation $P_t = V_t^2/Z$, where Z is the impedance in the circuit, and corresponding expression for P_r, with equation (2.5) the module then get the superposition voltage contribution amplitude from the transmission channel i to receiving channel j as

$$V_{j,r} = \sum_i V_{i,t} \sqrt{\frac{G_t G_r \lambda^2 \sigma}{(4\pi)^3 r_i^2 r_j^2}} \tag{3.3}$$

The impedances for transmitter and receiver are the same, since they use the same antenna, so they cancel out. This leaves the module to calculate which phase and delay the contribution should have. For this the total distance travelled from transmitter i to the target and then to receiver j is $R_{i,j} = r_i + r_j$ is used. Thus the time delay becomes $\delta t_{i,j} = R_{i,j}/c$.

The time delay is then used to correctly place the voltage data for each Rx-channel in the final matrix displaying the input voltages over time for each channel.

The way this is implemented in the simulation is illustrated in the sequence diagram in figure 3.8. That is that for every pulse we perform this operation for every target and superposition each contribution onto the same matrix with different scaling, frequency shifts and delays in order to create the full matrix of incoming voltages to the electronic simulation in each channel.

3.1.4 PeriodicInterferenceModule

The PeriodicInterferenceModule operates on the same principles as those of the PropagationModule described in subsection 3.1.3. The difference is that this module treats external sources instead of the transmitted radar pulse. Instead of target functions used in 3.1.3, the model uses PeriodicInterferenceSourceFunctions that, like the TargetFunction, returns the position and velocity of the external source. In addition it also returns

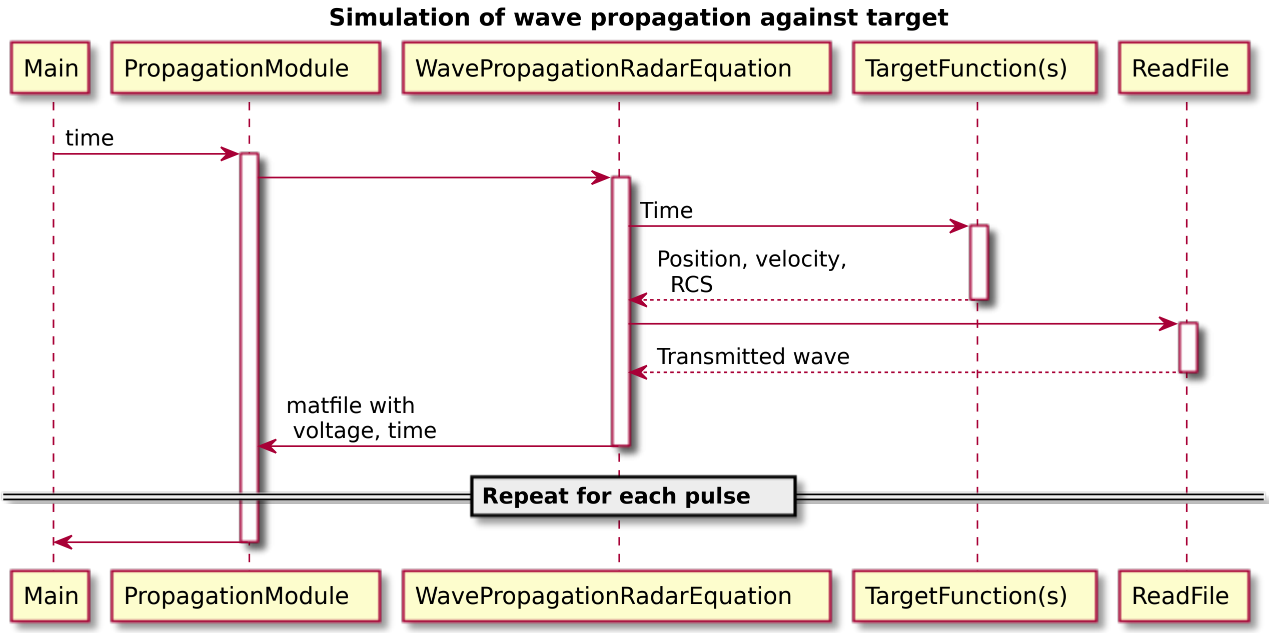

Figure 3.8: *The figures shows the sequence diagram of the propagation module.*

the waveform it transmits. This waveform is treated in the same way as in the PropagationModule with simplification to the voltage scaling from (3.3), due to that the wave only travels one way, resulting in(3.4).

$$V_{j,r} = \sum_i V_{i,t} \sqrt{\frac{G_r \lambda^2}{(4\pi)^2 r_j^2}} \tag{3.4}$$

3.1.5 EchoExtraction

Since performing electronic simulations is the most timeconsuming operation of the model, and the fact that for few targets we will have a propagation matrix which mostly consists of uninteresting noise information we easily find ourselves in a situation where we perform unnecessary circuit calculations. In order to save computation time we therefore extract the sections containing pulse data and form a second matrix consisting of all the concatenated pulse data as already illustrated in figure 3.4. This is then sent to the Rx module for simulation. Afterwards the processed matrix is again divided and inserted into the final output matrix.

During this operations we loose electronic simulation data of the background noise. In order to still incorporate this into the final product we process a small section of noise data in the Rx module and use this data to extract mean and deviation of the noise. These parameters are then used in ConcatenateRxOutput module to generate and filter noise to fill the gaps of data not simulated in VSS.

3.1.6 WavePropDisturbtionModule

This module has the function to add different kinds of noise to the system that occurs over the entire simulation run. The addition is performed to the parts of the matrix that has been extracted by the EchoExtraction module. The reason for this is to save computation time by decreasing the number of memory writes compared to implementing the noise addition using the PeriodicInterferenceModule.

3.1.7 RxModule

The RxModule operates using the same principles as those of the TxModule, described in subsection 3.1.2. The circuit of the receiver was modelled in VSS cascading a set of filters and amplifiers. The filters was designed as band pass filter with a band centred round the transmitted centre frequency of 1.3GHz. In order to model the non-linearity of the system we used a amplifier model with output vs input characteristics shown in figure 3.9, which is output is explained in section 2.3. Thus showing the same characteristics as shown in figure 2.4

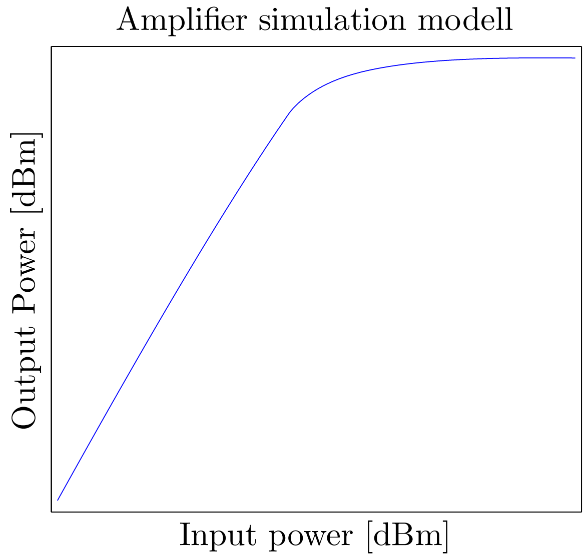

Figure 3.9: *The figure shows the output power of the simulated amplifier as a function of input power.*

Since the purpose is to study the effects of non-linearities the circuit was modelled to start with a filter and terminate with a amplifier to make sure the nonlinear components from a saturated amplifier is not filtered away at the output. yielding a design like in figure 3.10

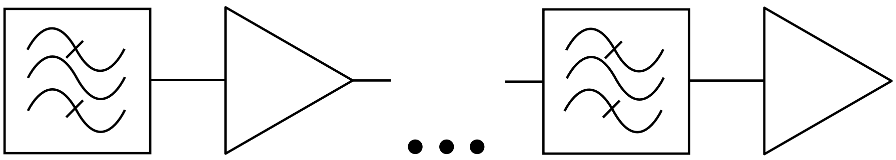

Figure 3.10: *The figure shows cascading of filters and amplifiers used in the electronic circuit.*

3.1.8 ConcatenateRxOutput

The ConcatenateRxOutput is essentially a module that performs the operation of EchoExtraction backwards, as illustrated earlier in figure 3.4. What it does is that it takes the noise data extracted from EchoExtraction and has been processed by the RxModule. It then uses this data to generate noise for the final matrix that later is to be sent to the SamplingModule. After this has been done it takes the data from the extracted echoes and insert them back to its proper place in the final matrix, replacing the generated noise at the position. The final complete matrix is then sent to the SamplingModule, explained in subsection 3.1.9.

3.1.9 SamplingModule

This module constitutes the beginning of the digital signal processing illustrated as point A in figure 2.3, which has the purpose to express the data from the 2D matrix returned by the ConcatenateRxOutputModule into a 3D matrix as detailed in figure 3.5. First the the implementation details will be treated and then the changes to the signal for each step will be presented.

The SamplingModule is a straight up implementation of the theory in section 2.5. First it samples the signal with 2^n levels in the voltage range $[V_-, V_+]$ using an ADC sampling frequency $f_s = 960$MHz, then it performs the conversion to base band and I/Q split using (2.40). Thereafter it performs the decimation utilising a Blackman-Harris filter [7] in accordance with equation (2.41).

Now the effect on the signal for each step will be presented. Starting with the input into the ADC in figure 3.11.

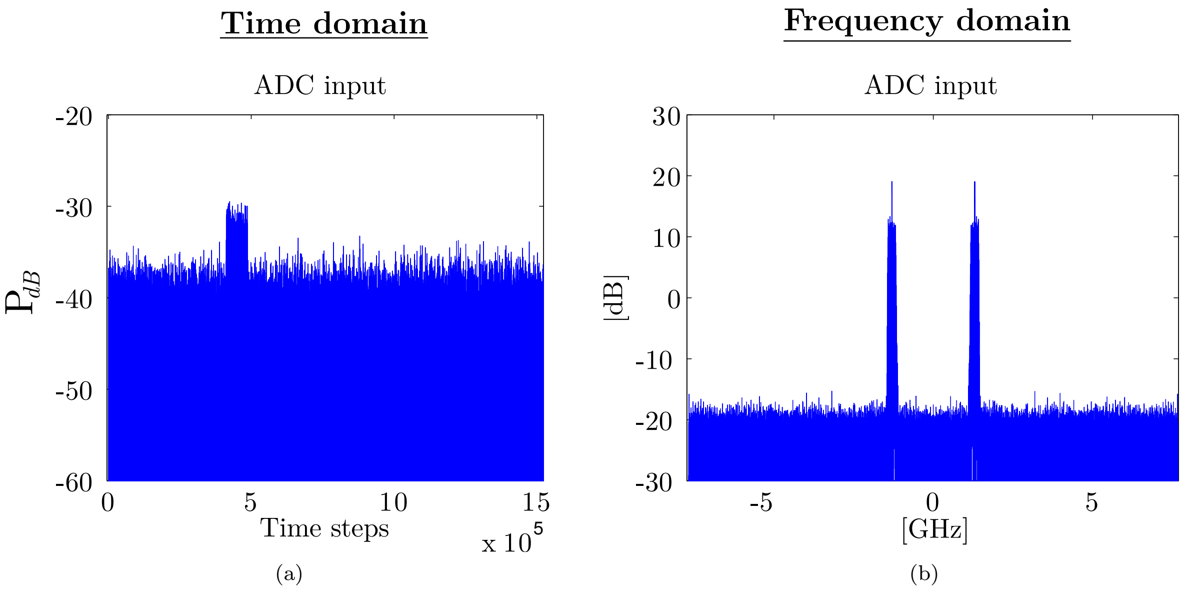

Figure 3.11: *The figure shows the signal appearance at point A in figure 2.3, which is the input to the ADC, from a clear echo. Figure 3.11a displays the input in time domain for one pulse and 3.11b illustrates the input in frequency domain. For the frequency domain the reference point is taken as the mean of the noise level in the receiver band when no signals enter the systems.*

As can be seen in the time domain for one pulse the amplified echo from the Rx is clearly seen above the noise. Looking at the frequency spectra in figure 3.11, three things can be seen. First the noise floor from the thermal noise at the end of the receiver. Secondly the amplified noise within the receiver band-pass filter and thirdly the signal standing out in the middle of the band-pass.

Letting this signal undergo the operations explained in section 2.5 results in the changes presented in figure 3.12.

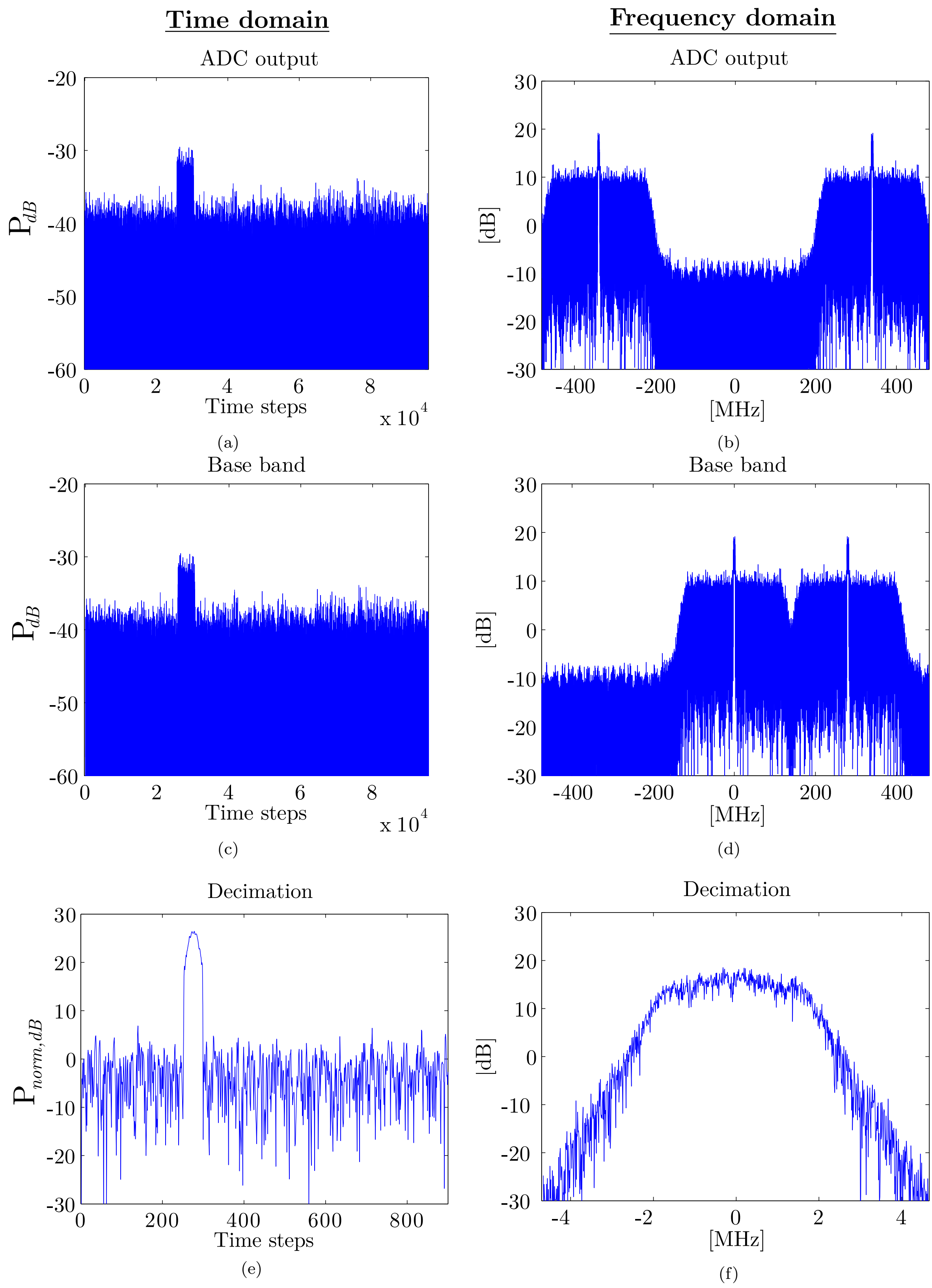

Figure 3.12: *The figures shows the signal at points B-D in figure 2.3 in the time domain for one clear pulse echo and its corresponding frequency spectrum as the different steps are performed by the SamplingModule. Figure 3.12a-3.12b shows the signal after it has been sampled by the ADC, 3.12c-3.12d shows when the signal band has been moved to baseband and 3.12e-3.12f displays the pulse after decimation, where time steps has been greatly reduced and the frequency spectra narrowed.*

From the figure it can be seen that the signal centred round 1.3GHz now has folded into 340MHz and that the noise level outside receiver band-pass has increased due to folding of external frequencies. Continuing on the signal is moved to baseband from its position at 340MHz. After the shift to baseband the signal then undergoes decimation leaving a time domain pulse with much lower number of time steps and where the signal band has been extracted.

The figure 3.12 showed a rather clear echo in order to easily follow the signal. In normal operation you often treat much weaker echo such as the one whose ADC input and sampling steps are presented in figure 3.13 and 3.14.

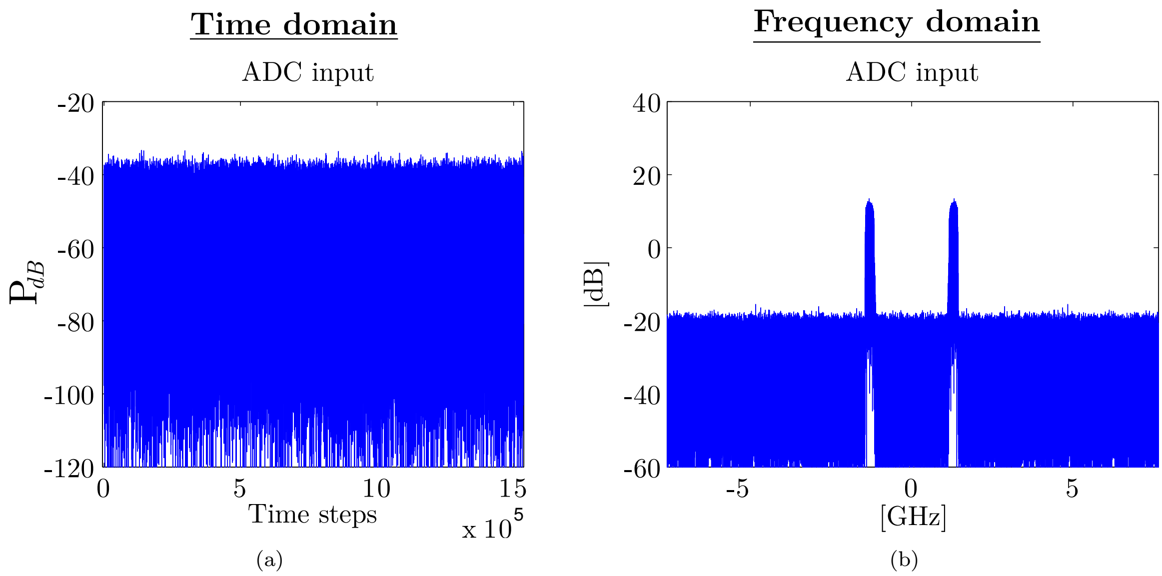

Figure 3.13: *The figure shows the signal appearance at point A in figure 2.3, which is the input to the ADC, from a small echo. Figure 3.13a displays the input in time domain for one pulse and 3.13b illustrates the input in frequency domain. For the frequency domain the reference point is taken as the mean of the noise level in the receiver band when no signals enter the systems.*

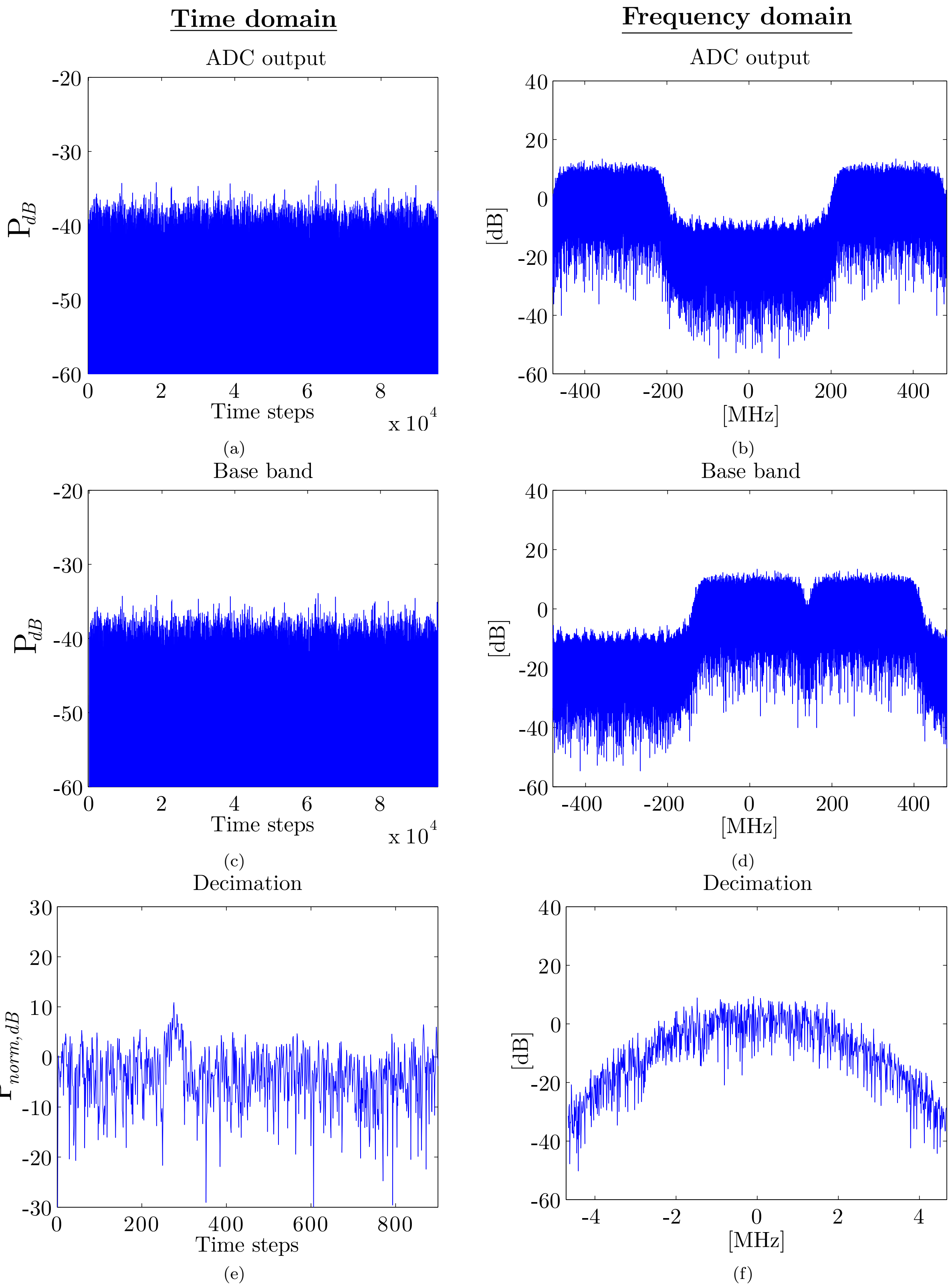

Figure 3.14: *The figures shows the signal at points B-D in figure 2.3 in the time domain for one small pulse echo and its corresponding frequency spectrum as the different steps are performed by the SamplingModule. Figure 3.14a-3.14b shows the signal after it has been sampled by the ADC, 3.14c-3.14d shows when the signal band has been moved to baseband and 3.14e-3.14f displays the pulse after decimation, where time steps has been greatly reduced and the frequency spectra narrowed.*

Here the signal is not to be observed until it barely can be seen after the decimation in the time domain, and often signals much weaker than this is treated making it indistinguishable from noise during these operations.

In addition to the appearance of the signal from the receiver during the sampling process it is of interest to observe how the sampling process looks when the input is ideal and noise free. This is realised by using the output from WaveFormMatGenerator as input to the SamplingModule. The results are presented for the frequency domain in figure 3.15. This final output is also the signal used to correlate the received signal during operation in the SignalCorrelationModule, treated in subsection 3.1.10. As can be seen this signal behaves in the same way as 3.12 .

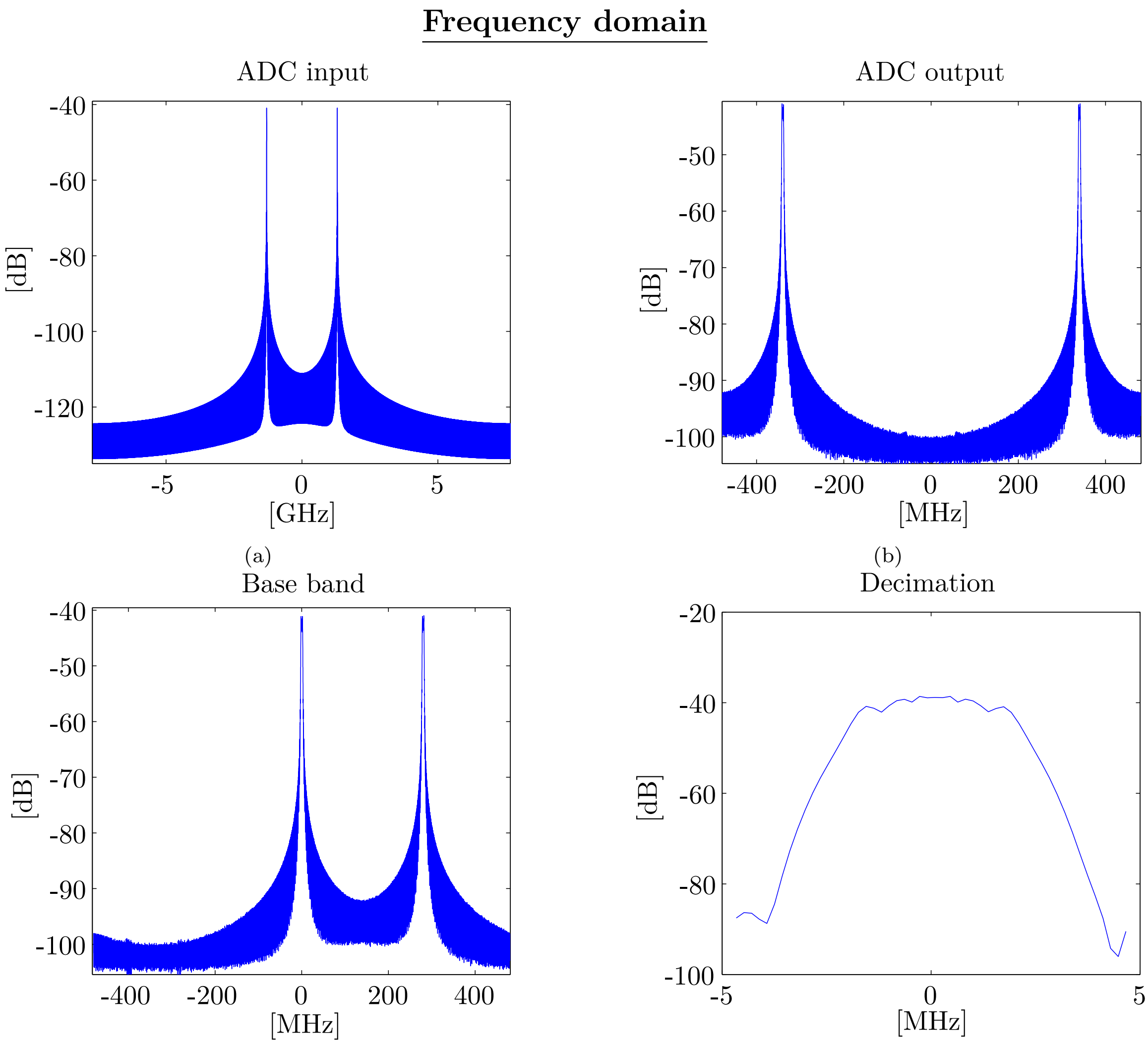

Figure 3.15: *The figures shows the power spectra for the different steps performed by the SamplingModule for an ideal noise free input consisting of one pulse. 3.15a displays the original signal, 3.15b shows the signal after sampling by the ADC, 3.15c displays the move to baseband and 3.15d shows the signal after decimation.*

3.1.10 SignalCorrelationModule

This module performs the pulse compression between point D and E in figure 2.3. The process is performed by correlating the transmitted ideal signal, presented in figure 3.15, with the incoming signal from point D. This process is illustrated using the different echo magnitudes from figure 3.12 and 3.14 in figure 3.16 and 3.17. Here it clearly can be seen how the power of the signal is concentrated in time and that there is an increase in the normalised power of the signal by about 12dB.

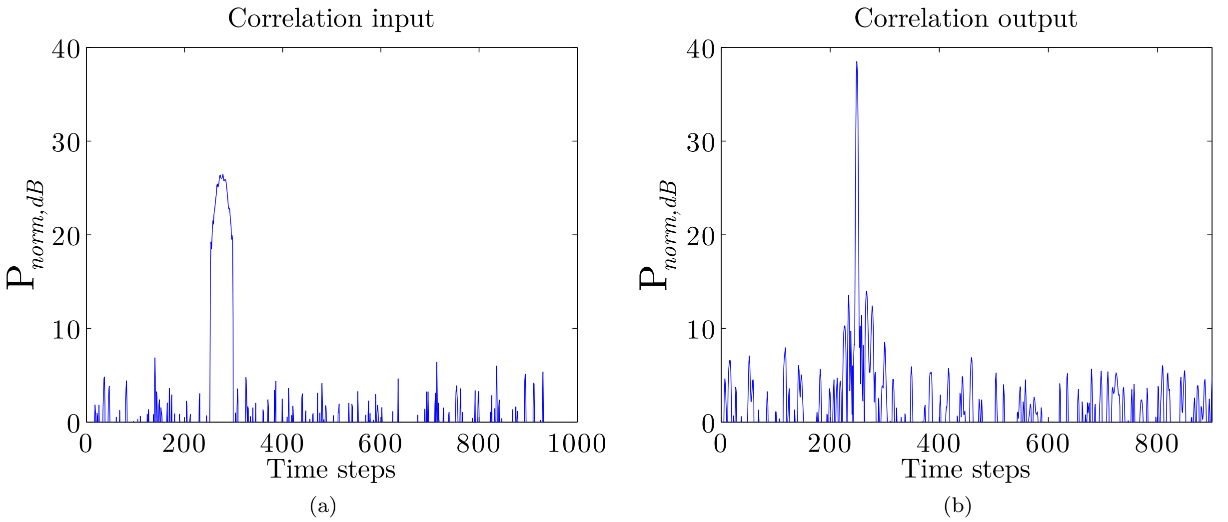

Figure 3.16: *The figure shows the correlation step performed on the clear echo presented in figure 3.12.*

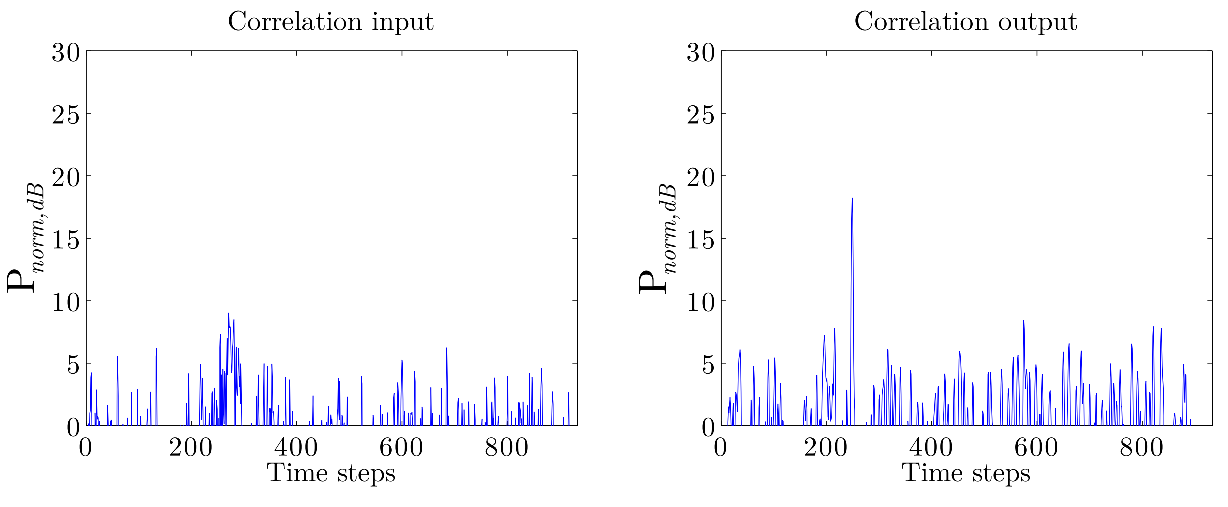

Figure 3.17: *The figure shows the correlation step performed on the small echo presented in figure 3.14.*

3.1.11 BeamFormingModule

Following the signal chain presented in figure 2.3, the next step is to perform the beam forming as detailed in section 2.6.1. The results of this operation on the signal from figure 3.12 is showed in figure 3.18.

In the figure one can see the main lobe at 60 degrees surrounded by its side lobes, indicating that the target that the target is positioned in that direction. As can also be observed the SNR_{dB} has increased by $10\log_{10}(nChannels)$ over the output of the pulse compression in accordance with expectations.

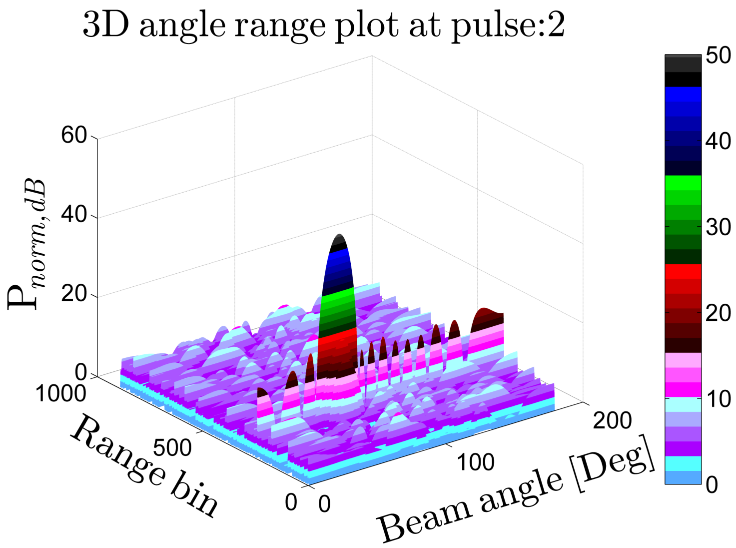

Figure 3.18: *The figure shows the target matrix representation after beam forming of one chosen pulse from the same case as that of figure 3.16, with one target at range bin 247 and direction 60 degrees.*

3.1.12 DopplerFilteringModule

This is the last module in the program structure, presented in figure 3.3, and performs the doppler filtering, which is the last operation of the DSP in this thesis. The step uses the multiple pulses to concentrate the energy in velocity space. The effect of performing a doppler filter process using 128 pulses of the signal in figure 3.18 is showed in figure 3.19.

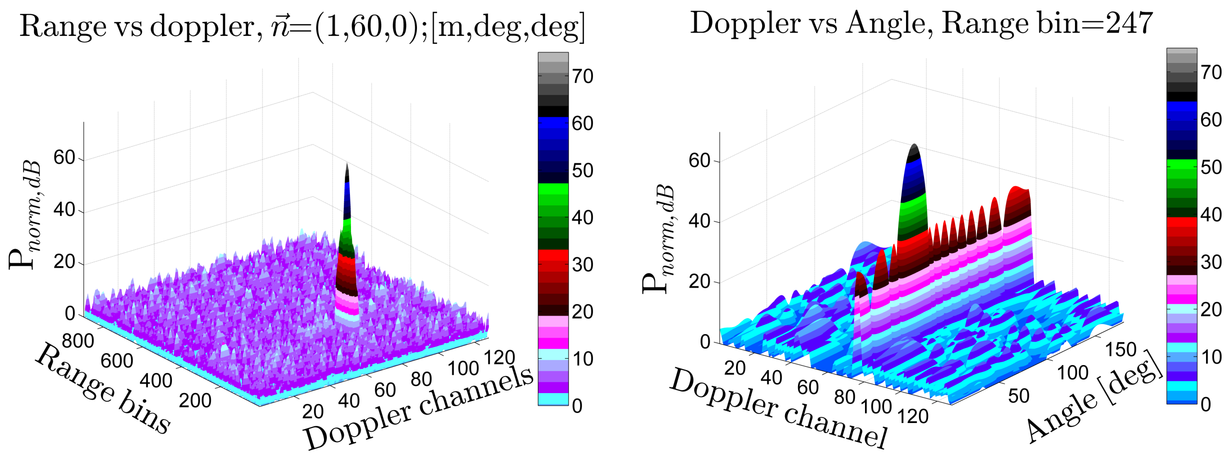

(a) (b)

Figure 3.19: *The figure shows the doppler filter results using the signal from figure 3.18, with a target at (4km, 60deg, 0deg) with a radial velocity of -100m/s. The target is followed over 128 pulses. Figure 3.19a and 3.19b shows the same scenario but fixing different dimensions in the detection matrix.*

By comparing the power peak of figure 3.18 and 3.19 we can see the expected signal power increase of $10\log_{10}(nPulses)$.

4 Results

In this chapter the results from the different simulation scenarios are presented. Each scenario will start with a presentation of the scenario and an explanation of the value of the results. Afterwards the results will be treated and following this there will be a discussion. All positions specified in this chapter is expressed in the inertial system defined in figure 3.7.

4.1 Single and multiple target detection under normal operation

The scenarios in this section presents results from a typical operation where non-linear effects has little to no effect on the results since the power of the input signal to the receiver is very low. The purpose of this section is to introduce the format of presentation and give some reference as to have a good scenario looks like in order to get a better understanding of the scenarios in later sections.

The first case is that of a single point clutter, equivalent of a stationary target, which after the signal processing chain has a normalised power of 37dB. The clutter is positioned at a distance equivalent to 497 range bins from the radar at angle of 90 degree azimuth, meaning straight forward in bore sight. Since the target is stationary it has zero radial velocity and the radar is transmitting at the same direction as the target. In order to visualise the detection, 2D cuts of the 3D matrix, illustrated in figure 3.5 are taken and displayed in figure 4.3. By looking at the peak in figure 4.3 the power peak from the clutter can be observed at range bin 497 at 90 degrees and doppler channel 65 corresponding to zero radial velocity.

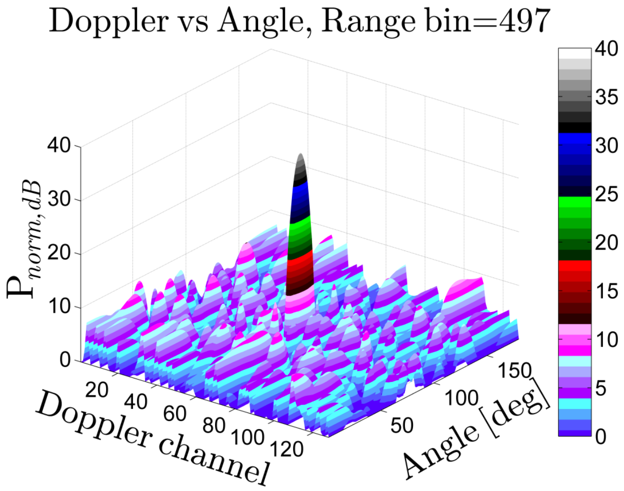

Figure 4.1

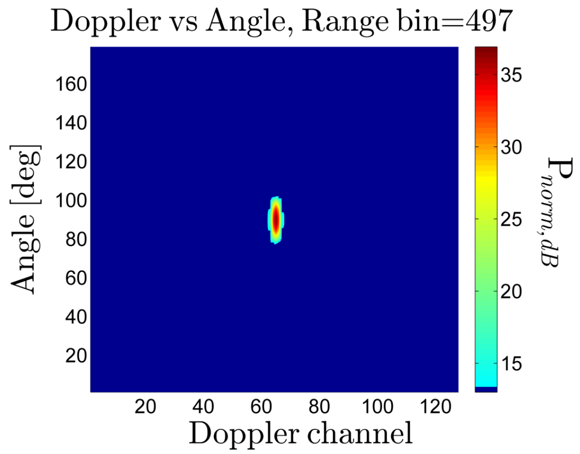

Figure 4.2

Figure 4.3: *The figure shows the normalised power, $P_{norm,dB}$ from the echo of a stationary target (doppler channel 65), with position (8km,90deg,0deg) corresponding to range bin 497, presented in 4.1. To the right in 4.2 the 2D projection of 4.1 where a detection threshold of 13 dB has been introduced is presented.*

In the same manner the peak can be confirmed to appear at range bin 497 by instead observing the range bins and doppler channels in the direction of 90 degrees azimuth, as presented in figure 4.4.

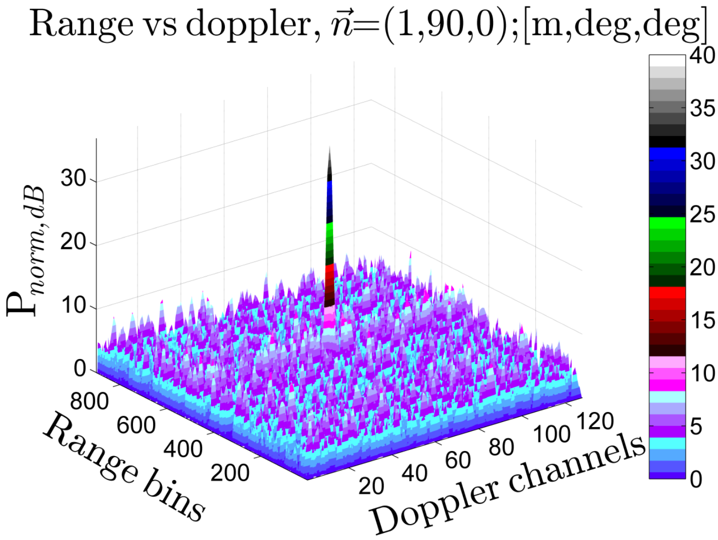

(a)

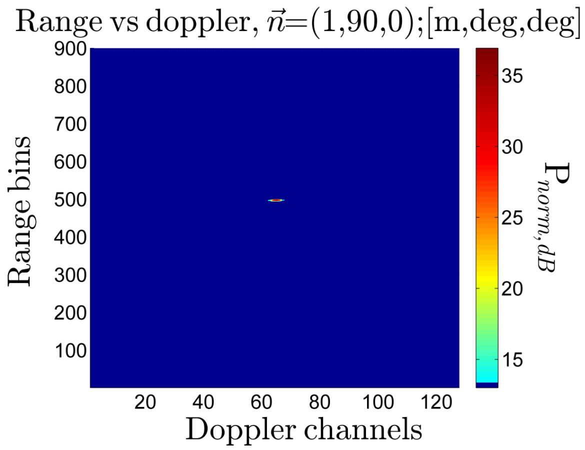

(b)

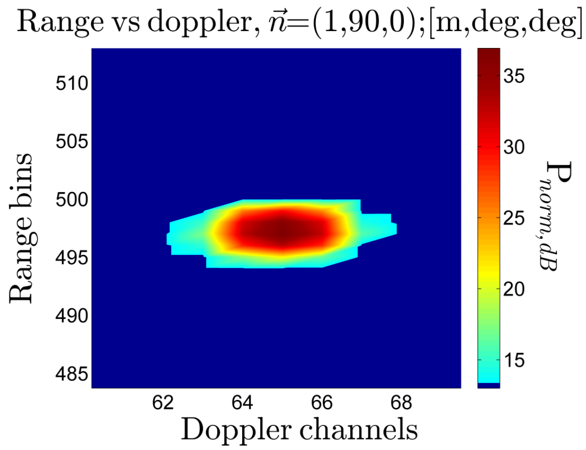

(c)

Figure 4.4: *Figure 4.4a shows the normalised power, $P_{norm,dB}$, at direction 90deg from a target at position 497 range bins and 90degrees azimuth. Below in 4.4b and 4.4c the 2D projection of 4.4a is presented when a detection threshold of 13 dB has been introduced.*

Knowing the position of the peak it is also possible to observe the cuts along each separate matrix dimension intersecting the power peak as is presented in figure 4.5.

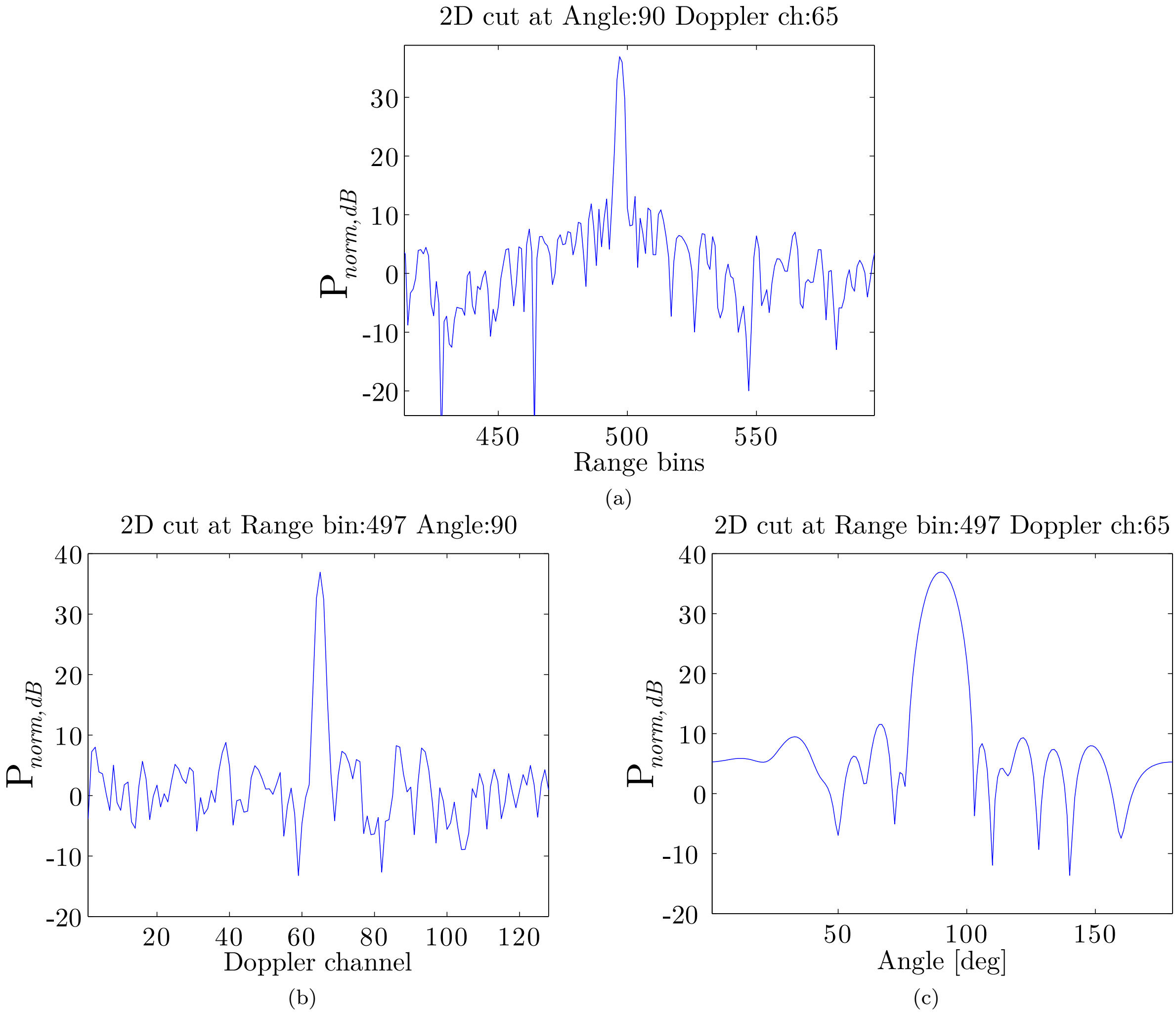

Figure 4.5: *The figures 4.5a- 4.5c shows 2D cuts intersecting the power peak of the target echo for a target, with final normalised power of 37dB, at range bin 497, angle 90deg and doppler channel 65.*

Having observed the appearance of a stationary target, the difference introduced by exchanging the stationary target to two moving targets with equal RCS can be observed in figure 4.6. Here both targets has been placed at the same distance from the radar but at angle 60 and 90 degrees azimuth respectively. The target at 60 degrees has been given a radial velocity of -100m/s while the target at 90 degrees was given a radial velocity of +200m/s. From figure 4.6 both targets can be observed at angle 60 and 90 degrees. The one at 90 degrees have a much lower normalised power since the radar is transmitting in the direction of 60 degrees azimuth. As should be expected the detection with the highest normalised power is the target positioned in the direction of the transmitted direction of the radar. The target is also sorted into doppler channel 76, corresponding to -100m/s. The other target at 90 degrees is instead sorted into doppler channel 43 twice the distance from channel 65 then the other target peak and it therefore corresponds to a radial velocity of 200m/s.

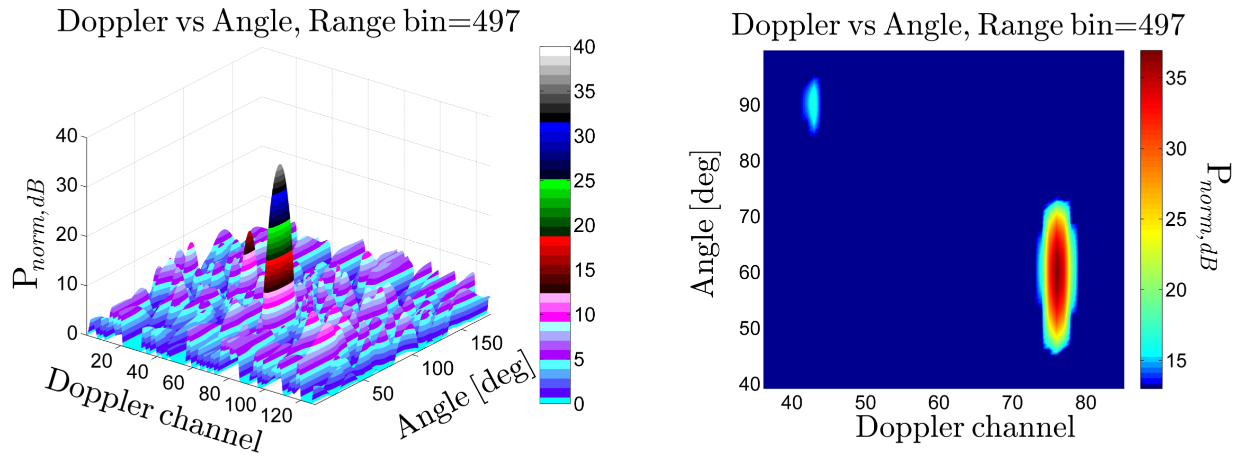

(a)

(b)

Figure 4.6: *Figure 4.6a shows the SNR_{dB} vs angle and velocity at range bin 497 and 4.6b shows the corresponding 2D projection of 4.6a when a detection threshold of 13 dB has been applied.*

From these results we can see that during undisturbed operations at this distances there is no problem to discern the location of the target in the 3D detection matrix. We can also clearly see the effect the direction of the transmission has on the final power level of the target by observing figure 4.6b. Here a power difference of about 20dB can be observed between being illuminated in the transmission direction and 30 degrees away from the transmission directionin. Another thing to note is that the width of the main beam along the azimuth dimension corresponds to that of the theory in section 2.6.1.

4.2 External noise jammer

Building on from the results from normal operation presented in section 4.1 this section shows the effect that a noise jammer has on the detectability of a target when the jammer operates in the radars sampling band. This is to illustrate the basic effects that increased noise has on the system.

In this scenario the noise jammer will consist of pulsed normal distributed noise, uncorrelated between the pulses, which simulates a CW noise jammer when the PRF of the jammer corresponds to the PRF of the radar. Since the jammer signal consists of noise, it will receive no signal increase from the pulse compression since the noise doesn't correlate with the radar signal. Given that the noise doesn't correlate between pulses, or as a CW signal, it will neither experience amplification from the doppler filtering. Since the jammer transmits from a stationary point however the jammer signal will become amplified by both the electronic amplifiers and the beam forming process. The effect observed is that the noise floor surrounding the target peak has a higher value then the noise level during normal operation which in turn results in a need for a higher signal power in order to pass the threshold. This is illustrated in figure 4.7 where a noise jammer in direction 60degree azimuth overlaps the echo from the target at position range bin 249.

From this results we can see that the presence of noise in the sampling band decrease the detectability of the target where strong enough noise will drown the signal of interest. This is the same thing that occurs in traditional radar and comes as no surprise.

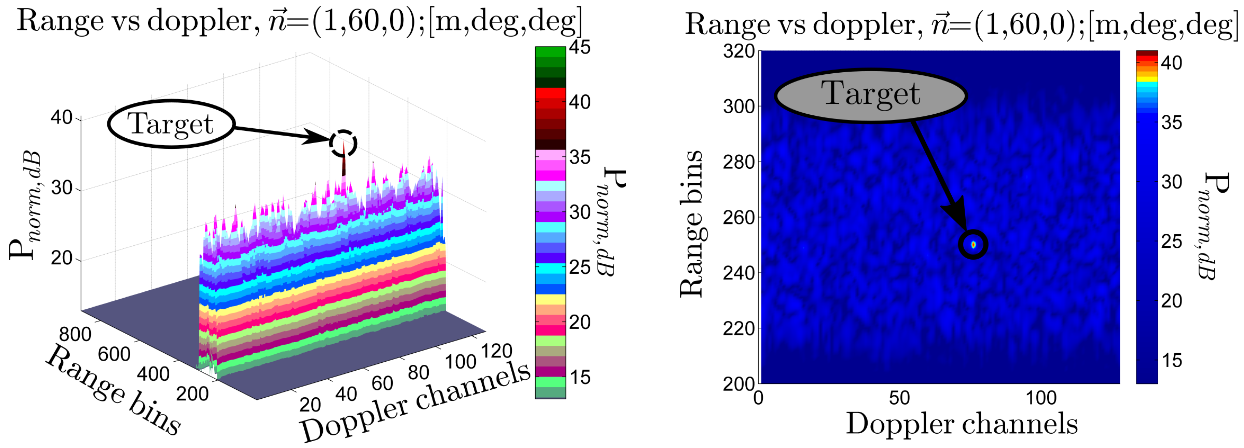

(a)

(b)

Figure 4.7: *Figure 4.7a signal strength vs doppler channel and range for a case when a target echo is overlapped by a noise jammer. The target signal has a final normalised power,* $P_{norm,dB}$*, of 42dB and a radial velocity of -100m/s, corresponding to doppler channel 76, at range bin 247 at direction 60deg. The noise jammer transmits pulsed white noise which totally covers the target echo. In figure 4.7b a 2D projection of 4.7a is shown when the threshold has been increased to discern the target peak.*

4.3 Effects on final signal power from increasing input power to the receiver

This section treat the impact on detectability of a target when an external signal is saturating the amplifier circuit and moving further into the compression region earlier presented in figure 2.4. This is interesting since it demonstrates how well an unshielded system can detect a target, when its subject to strong interference inside its analogue band. This thesis will treat two scenarios. The first is the saturation due to a strong point clutter, and shows the effect when the same wave form as the one the radar transmits saturates the system. The other is when the source of the compression is external and utilises another waveform, sending at the same PRF as the radar, but at a different centre frequency that still lies within the analogue band of the receiver. This is especially interesting since this is testing the selectivity that has been sacrificed due to the simpler circuit design at detailed in section 2.1.

The first scenario, containing the point clutter, is constructed by placing a target with -100m/s radial velocity at 60 degrees azimuth so that the final normalised power after the signal processing becomes 48.5dB. The clutter is placed at 90 degrees azimuth at a slightly longer radial distance so that the overlap between the target and clutter echo are 93% in the time domain. Then multiple simulation runs are performed where the RCS of the clutter is increased, resulting in a higher input power to the system. The power sweep showing the peak values of both the target signal and the clutter in the 3D detection matrix is presented in figure 4.8.

In this figure the effects of the non-linearity can clearly be seen once the input power from the clutter becomes strong enough to reach the output power P_{1dB} at the last amplifier, presented by the dotted vertical line. The C curve acts just like the model for the amplifier presented in figure 3.9. The S level of the target also remains constant until the amplifier starts to go into compression and once the saturation starts the S drops. It can also be seen that the power loss for S is close to that of C when comparing to the ideal linear response.

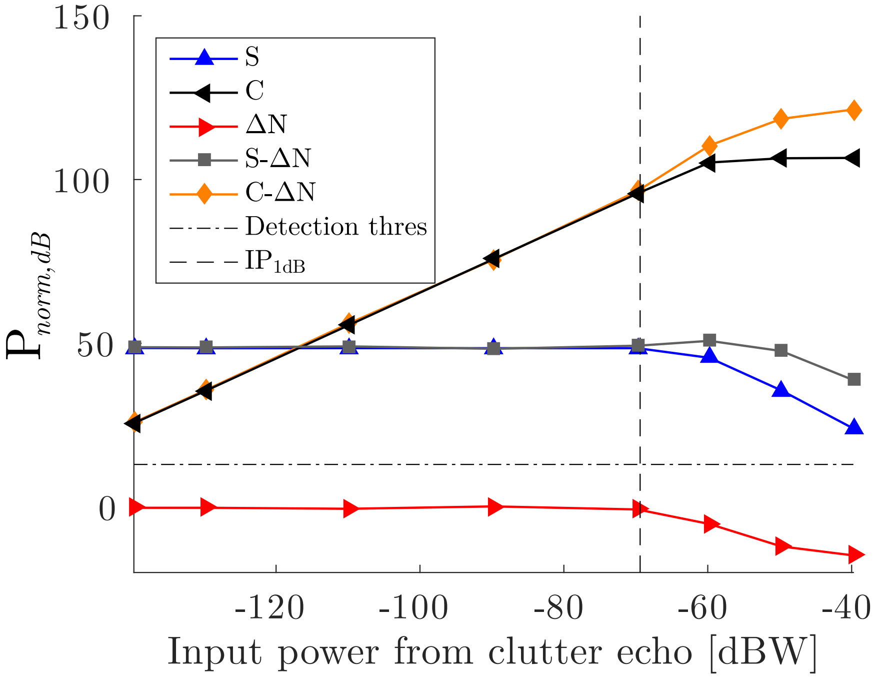

Figure 4.8: *The figure shows the normalised power, $P_{norm,dB}$ for the target signal, S, position together with the maximum power peak of the clutter, C, ΔN denotes the deviation of the local normalisation level round the signal from the case with no incoming signals. A negative value means that the noise level is lower due to compression. Marked in the figure is also a detection threshold of 13dB and the power level at which the input power from the clutter reaches P_{1dB}.*

For the second scenario the clutter is replaced by an external jammer. The external jammer transmits an linear chirp with the same bandwidth and PRF as the radar but at a different centre frequency. The centre frequency of the jammer was chosen by observing figure 4.9, which is extracted from figure 2.7, first presented in section 2.5.1. The centre frequency was chosen to 1.33GHz, to avoid the folding of higher harmonics into the radar's sampling band, while still being inside the analogue filters of the receiver.

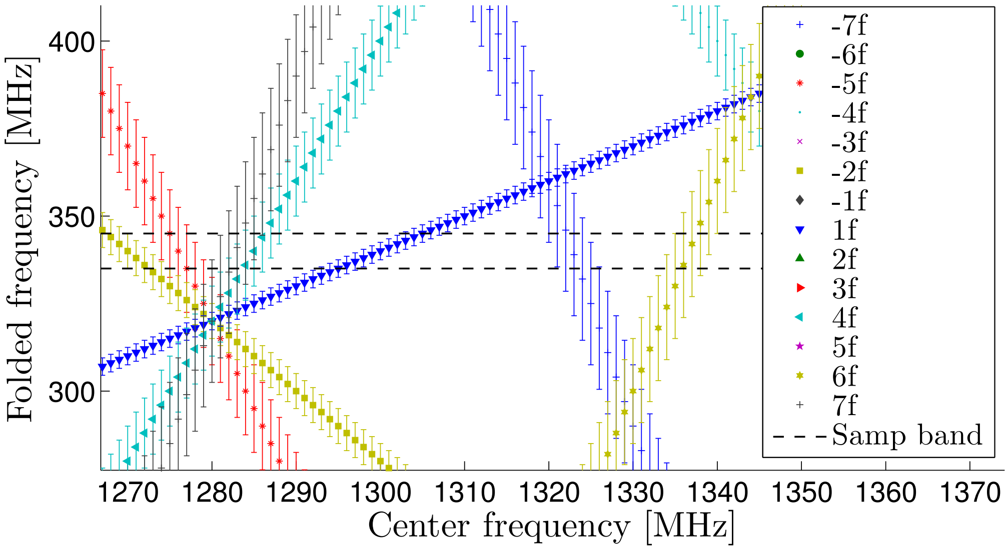

Figure 4.9: *The figure shows a magnification of a piece of figure 2.7 where the frequency placement of folded harmonics from a 5 MHz bandwidth centred round different frequencies are displayed when under sampled with a sampling frequency of 960MHz. This figure is zoomed in at the bandwidth which is sampled during the decimation that takes place between C and D in figure 2.3. The sampled band is positioned between the dashed lines.*

Apart from the centre frequency the jammer operated in the same way as our system and was transmitting from angle 90 degree azimuth with a delay so that the overlap between the jammer signal and the target echo was 93%. The power sweep showing the peak power of the target signal and jammer in the 3D detection matrix is presented in figure 4.10

As can be seen from the figure, the jammer does presents itself after the signal processing. Contrary to what was expected. The reason for this is due to spectral leakage of the jammer and will be explained in section 4.4. Should the signal not exhibit the this spectral leakage the appearance of J in figure 4.10 would disappear but the behaviour of S would be unchanged.

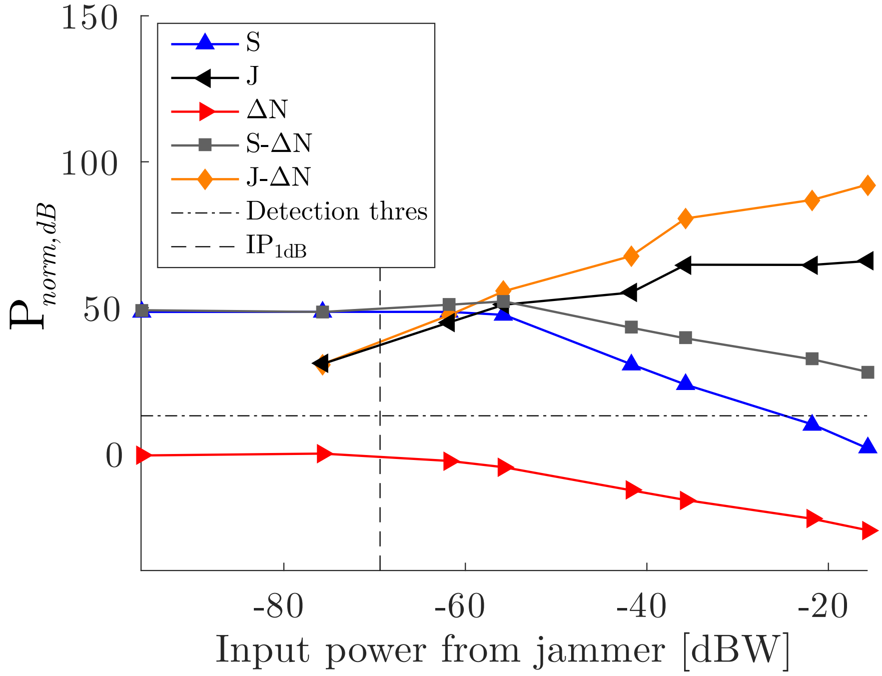

Figure 4.10: *The figure shows the final normalised power $P_{norm,dB}$ of the target signal, S, together with the peak jammer power, J, in relation to the normalisation level when there are no incoming signals. The jammer transmits a linear chirp with 5MHz bandwidth at centre frequency 1.3GHz+30MHz and the x-axis shows the input power to the radar receiver from the jammer signal. ΔN denotes the deviation of the local normalisation level round the signal from the case with no incoming signals. A negative value means that the noise level is lower, due to compression. Marked in the figure is also a detection threshold of 13dB and the power level at which the input power from the jammer reach P_{1dB}.*

The strength of J is lower then that of C in figure 4.8 at the same input power but the general trend is the same. The reason that J is lower comes from that the jammer isn't amplified during pulse compression, since it has another waveform, and the main bulk of the jammers power is outside the sampling band and is heavily suppressed during the decimation.

An important thing to observe is that the strength of the signal, S, decreases in the same way in both 4.8 and 4.10 since both the power from the jammer and the clutter passes the analogue filters and saturates the signal. This is an effect that would not have been observed for the jammer in a traditional radar, where the analogue circuit would have removed the jammer signal earlier.

Another thing to mention is that although the waveform used by the jammer in this section was a linear chirp, the results from this section can also be used for a case of a noise jammer with uncorrelated noise at the same bandwidth as the chirp. The difference this would make is that the noise would not be amplified by the doppler filtering, given that it is uncorrelated. Since neither the jammer chirp nor noise correlates with the transmitted radar signal neither of them will be amplified by the pulse compression. However the chirp might experience some shaping of the signal during the pulse compression, which the noise should not experience, if some part overlaps the sampling band. This is showed in figure 4.15 in section 4.4.

4.4 ADC clipping affects on signals

Following the results in section 4.3, this section treats the effects of clipping of the signal in the ADC as well as effects of type of signal that is forwarded to the ADC. This is important in order to understand the effects of different waveforms and operating frequencies as well as to explain the appearance of the jammer in the detection matrix in section 4.3.

To illustrate the effects of the ADC clipping the frequency spectra of the ADC input and the sampled signal will be presented, using a pulse that saturates the amplifier, from the jammer scenario in section 4.3 with a jammer centre frequency of 1.3GHz+30MHz that is sending a linear chirp with 5MHz bandwidth with the same PRF as the radar. Firstly the frequency spectra of the input signal to the ADC and the frequency spectra of the sampled signal without ADC clipping is presented in figure 4.11

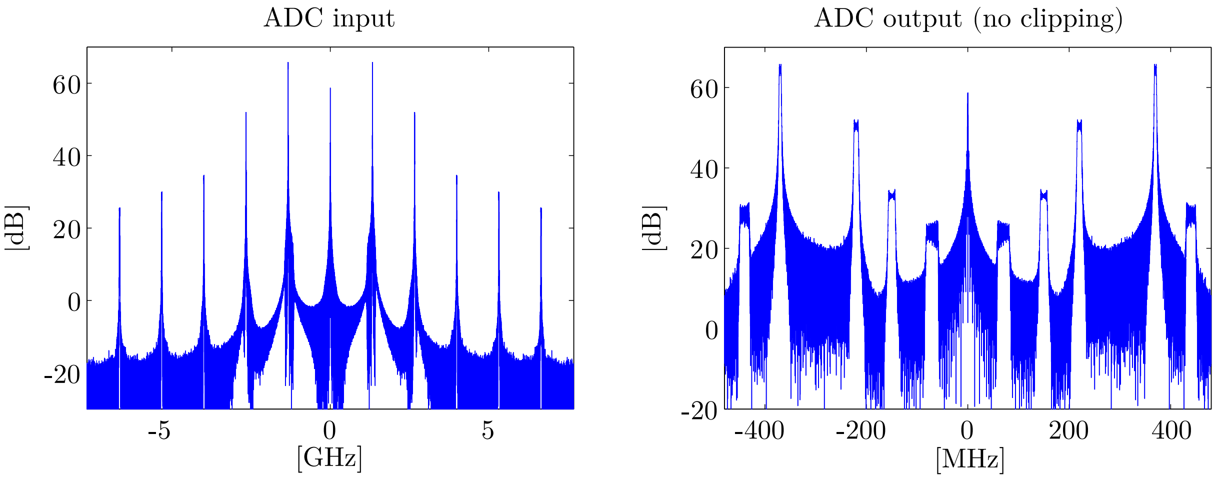

(a) (b)

Figure 4.11: *The figure shows the frequency spectrum of the input signal to the ADC, 4.11a, and 4.11a shows how the spectra of the sampled signal appears if the ADC has infinite dynamics and doesn't saturate.*

From the figure the harmonics generated by the saturation of the signal in the receiver is seen in the ADC input together with a DC component, which has it's origin in the two tone expansion of the fifth order polynomial as seen in appendix A. Upon sampling with the sampling frequency of 960MHz the harmonics are folded onto the band specified in figure 2.7, with each order of harmonics having equal wider band coverage. Since the ADC doesn't clip the signal the different band doesn't suffer any loss of strength as can be seen by comparing the heights in 4.11.

By comparing figure 4.11 with figure 4.12, which presents the frequency spectra av the sampled signal with clipping of signal, certain observations can be made. The clipping of the signal lowers the strength of the band of the input spectra and new bands appear. This is in accordance with the expectations from section 2.5.1. Since the saturation of the amplifiers generate both even and odd harmonics the clipping of these signals results in odd and even harmonics of the original signal band, even given the fact that the clipping itself only generates odd harmonics.

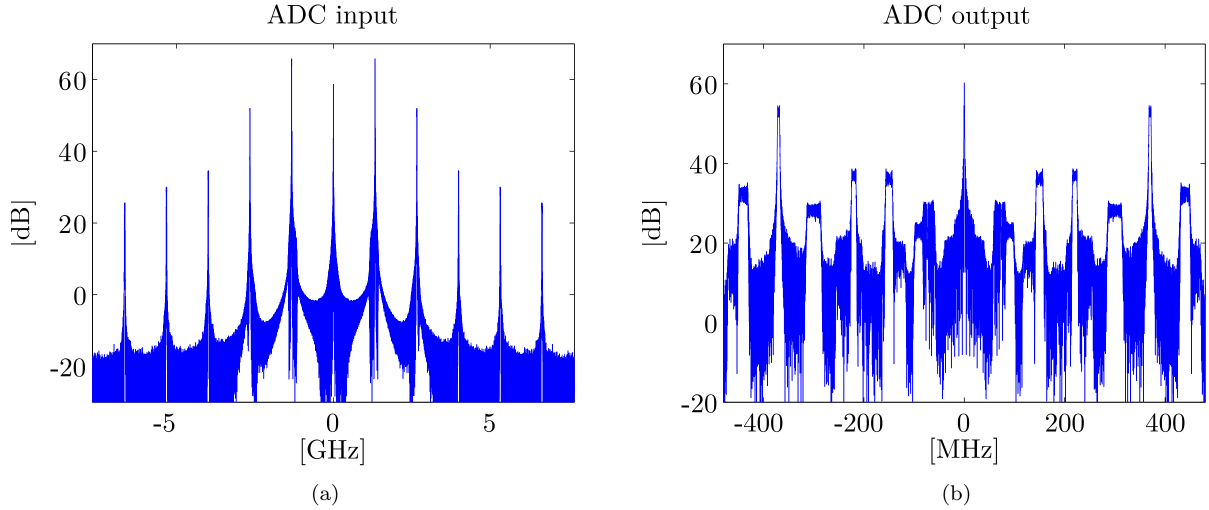

Figure 4.12: *4.12a shows the frequency spectra of the input signal to the ADC and 4.12b shows how the spectra of the sampled signal appears when the ADC clips the signal outside it's dynamic range.*

The effect of the clipping is easier seen by study the effects when the ADC input signal is filtered to remove the higher order harmonics as presented in figure 4.13 and 4.14.

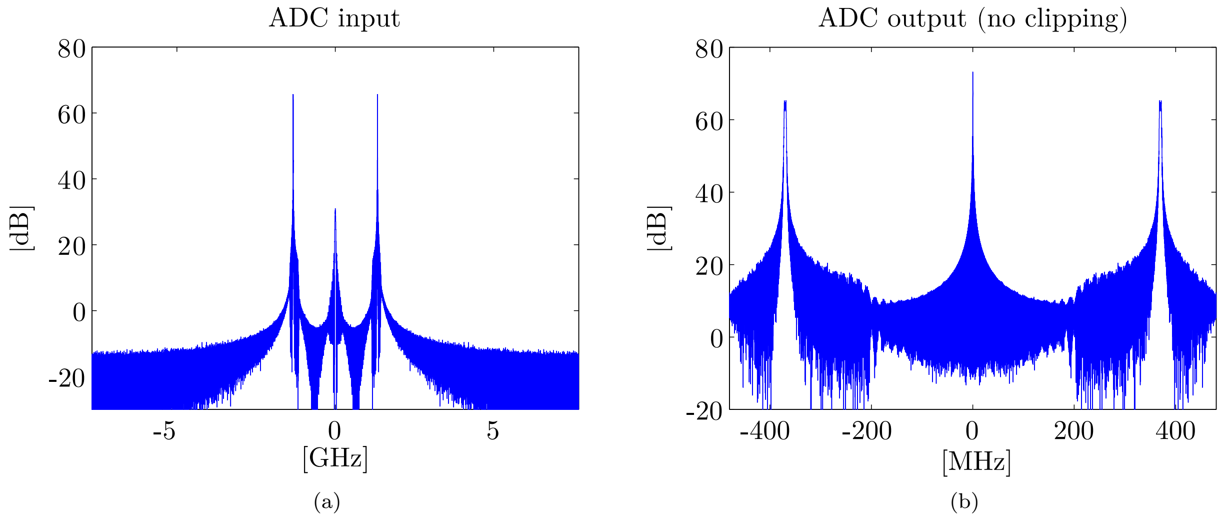

Figure 4.13: *Figure 4.13a shows the frequency spectra of the input signal to the ADC, when higher order harmonics has been filtered out, and 4.13b show the spectra of the sampled signal if the ADC has infinite dynamics and doesn't saturate.*

As seen in figure 4.14 the ADC clipping generates a frequency spectra much similar to that of figure 4.12.

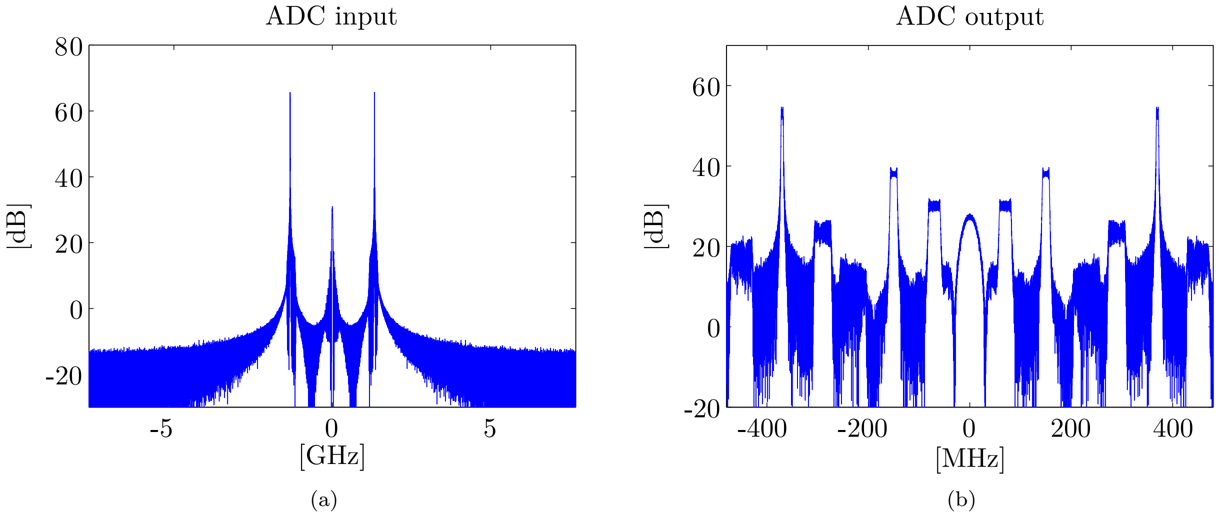

Figure 4.14: *Figure 4.14a shows the frequency spectra of the input signal to the ADC, when higher order harmonics has been filtered out, and figure 4.14b shows the spectra of the sampled signal when the ADC clips the signal outside the ADC's dynamic range.*

The effect of the ADC clipping also effects the signal after decimation as is showed in figure 4.15 and 4.16, where the input and output of the pulse compression with and without ADC clipping is showed. As can be observed the effect is a loss of power and a noisier signal. Since the signal used has another centre frequency then the signal used for the correlation it can also be observed that the signal experiences a decrease in SNR from the pulse compression, as well as a smearing of the peak. But as observed in section 4.3 the jammer signal still passes the filter operation.

Spectral leakage

Another observation to be done is that the filtered signal from the jammer with this particular waveform produces two peaks in the time domain, which then is smeared during pulse compression. This means the jammer signal will give rise to two detection in the range dimension, and since the jammer doesn't correlate with the transmitted signal of the radar the position of the peaks doesn't correspond to the correct time placement of the jammer pulse.

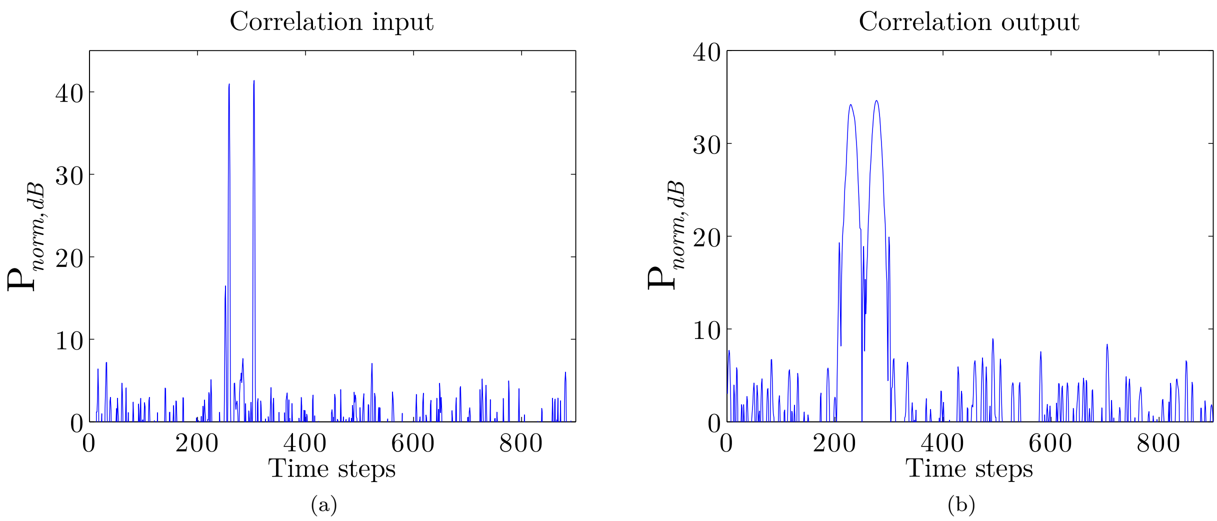

Figure 4.15: *Figure 4.15b shows the correlation output of the signal in 4.15a, previously presented in figure 4.11.*

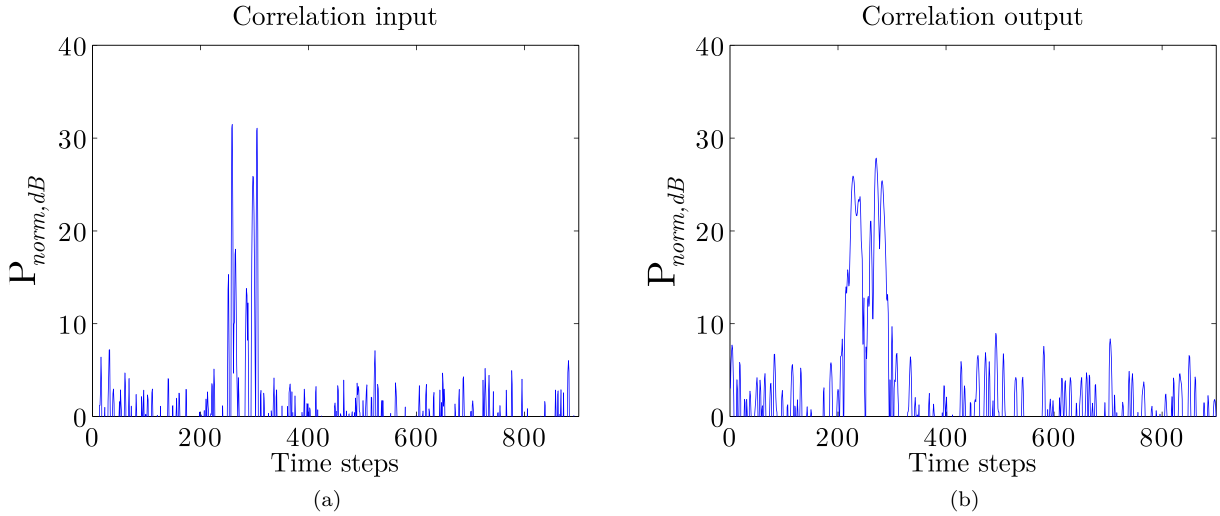

Figure 4.16: *Figure 4.15a shows the correlation output of the signal in 4.15b, previously presented in figure 4.12.*

The reason that the jammer passes the filter operation is made clearer by observing the part of the base band that is to undergo decimation, showed in figure 4.17

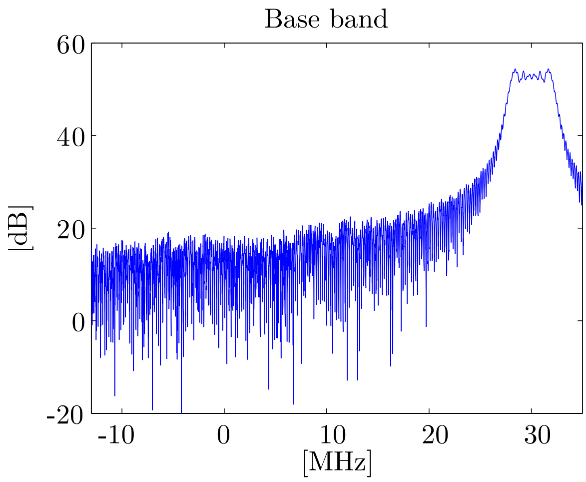

Figure 4.17: *The figure shows part of the spectra from figure 4.12 after the signal has been moved to base band.*

From the figure it can be seen that the signal exhibits quite big spectral leakage with a tail from the centre band of the jammer being observed spreading out over the band that is to be sampled. This is the reason for the appearance of such a strong signal. By instead using a signal with lower spectral leakage, presented in figure 4.18, the spectra appears much clearer and by observing the final band in figure 4.19 it can be seen that the tail is removed.

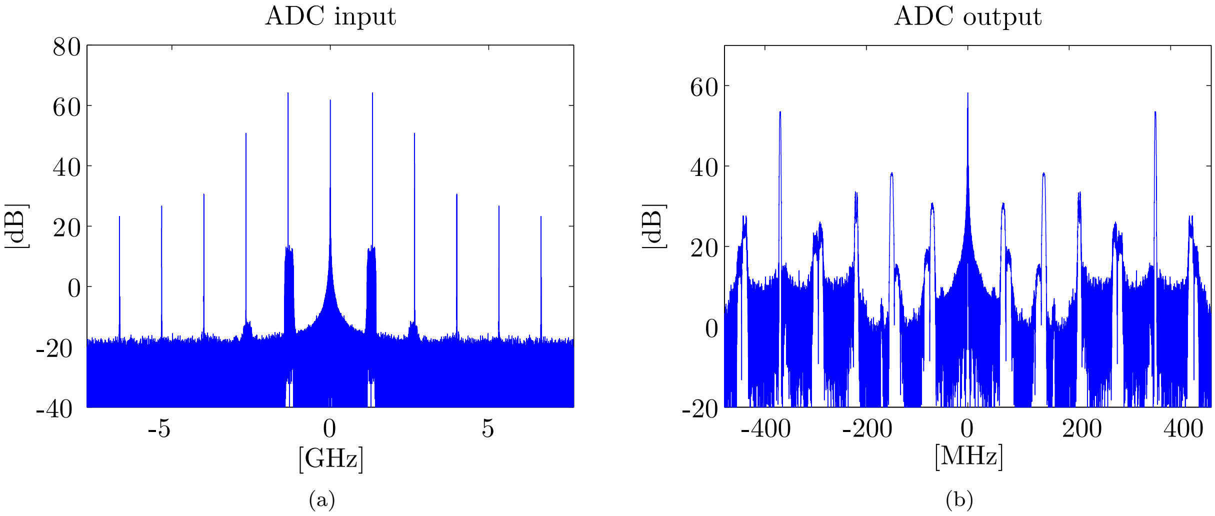

Figure 4.18: *The figure shows the same kind of scenario as figure 4.12 with the difference being that the external signal has been tapered to suppress spectral leakage. 4.18a shows the frequency spectra of the input signal to the ADC and 4.18b shows the spectra of the sampled signal when the ADC clips the signal outside the ADC's dynamic range.*

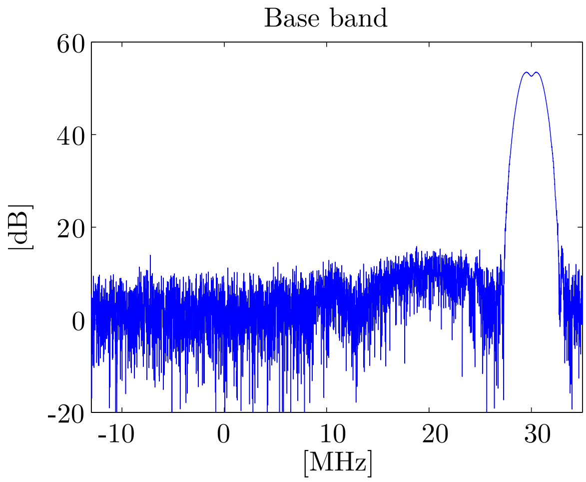

Figure 4.19: *The figure shows the same scenario as figure 4.17 with the difference that the external signal has been tapered.*

The effect from the spectral leakage is clearly demonstrated by observing the signal in the time domain during pulse compression as presented in figure 4.20, where the traces of the jammer that was seen in the untapered case in figure 4.16 now is gone. Even after beam forming and doppler filtering the jammer is not observed, which was what was originally expected in the sweep in figure 4.10.

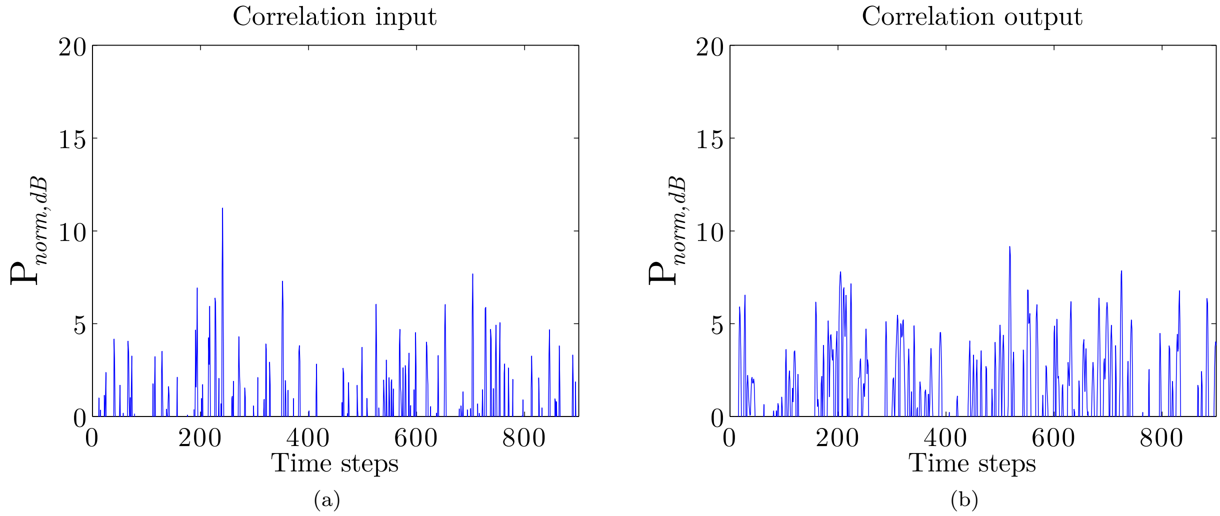

Figure 4.20: *Figure 4.20b shows the pulse compression of the signal from figure 4.18, where the spectral leakage of the signal has been suppressed.*

The important observation of this section is that the removal of external signals during decimation do work, as long as the external signal doesn't overlap the final sampling band. Another is that the clipping of the signals in the ADC results in a loss of power for the signal if the input to the ADC is to high. Lastly, due to the clipping external signals with harmonics that coincides with sampling band will fold into the sampling band if the external signal is high enough. These harmonic components still would have a waveform that doesn't correlate with that of the radar, so they should not receive any amplification during the pulse compression. It can also be noted that what we see here for the external chirp also can be applied to an external noise signal in the same frequency band, but the noise will not be amplified during the doppler filtering i f the noise is uncorrelated. It will neither be amplified during the pulse compression, since it doesn't correlate with the radar pulse.

4.5 False detections during saturation

In this section the appearance of false detections appearing in the 3D detection matrix in saturation scenarios will be treated in separate subsections. This in order to illustrate the composition of the detection matrix and compare scenarios when the saturation is caused by a strong clutter and an external signal like the one used in section 4.3. This is interesting because it gives a full understanding of how the data manifests itself in the detection matrix during saturation.

4.5.1 False detections from external jammer

The previous result sections briefly touched the subject of false detections by observing that the pulse compression of an external jammer signal, which doesn't correlate with the transmitted signal of the radar, can result in multiple false detections along the range dimension. Since this is an external source there is also not possible to ascertain the distance to the jammer purely by observing the delays between the jammer pulses.

Observing the result with spectral leakage from figure 4.17 and looking at the this scenario in the final 3D matrix, described to the lower right in figure 3.5, results in figure 4.21. Here a detection is drawn when the normalised power at a point in the matrix is above a 13dB threshold.

Here the two distance peaks seen in the pulse compression in figure 4.16. The reason why we see this uncompressed detection from the jammer signal is since the waveform of the jammer doesn't correlate with the transmitted signal of the radar. Extending from this jammer ridge along the range bin dimension, detections in the angle dimension extending from the higher values of the jammer ridge can be seen. These detections comes from the sidelobes of the beam forming since the array factor with this number of elements and tapering is unable to fully suppress the sidelobes. The detection of the target is seen as the detection breaking the periodicity, and is marked in the middle of the figure. However one can also see the appearance of new detections

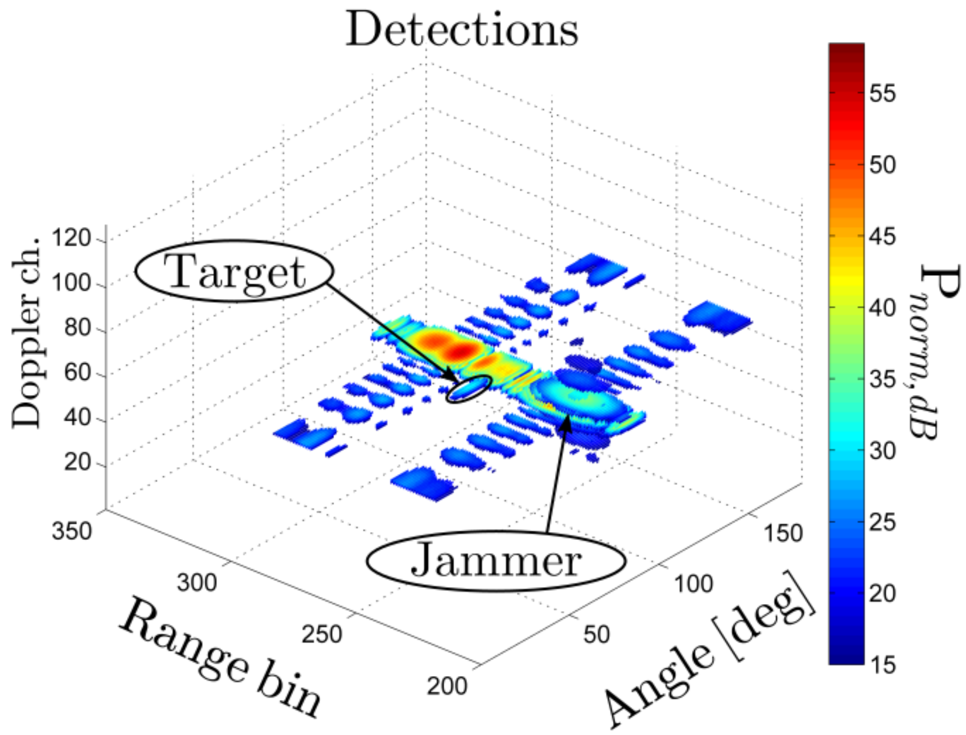

Figure 4.21: *The figure shows the detections in 3D detection space for saturation with a signal 30MHz above the radar signal band that saturates the amplifier.*

in the doppler dimension specifically round the nearest and most strong peak from the jammer.

If one instead observe the case when the jammer has lower spectral leakage, as presented in figure 4.22 one can observe that most of the detections has disappeared due to the lower strength of the jammer signal in the final band. Since the jammer with lower spectral leakage has a somewhat different waveform some small deviation in the appearance of the jammer detection along range dimension is seen. The target is detected at the same position but is a little clearer when compared to the surrounding. The target still has about the same power in both 4.21 and 4.22, but due to a slightly lower suppression of the signal we can also observe side lobes along the range dimension for the target. This is due to that the tapering during the pulse compression hasn't suppressed the side lobes below the detection threshold.

From this section we can see that when the system becomes saturated, the power level has become so high that the suppressed side lobes in the different dimensions of the detection matrix still appear above the used threshold of 13dB. The position on the sidlobes along the angle dimension are easily predicted since they comply with those of the array factor from figure 2.10. The other however aren't as easy to predict, since it depends on the correlation between the transmitted waveform from the radar and that of the jammer. As for the side lobes along the doppler dimension, they depend on the velocity of the target, which will be further treated in subsection 4.5.3.

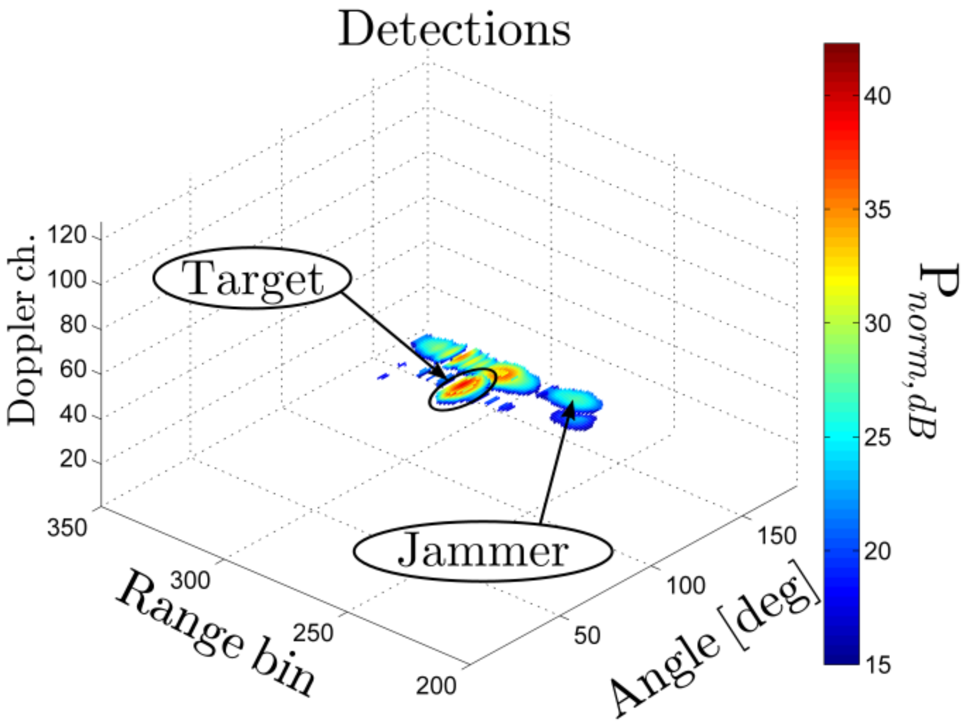

Figure 4.22: *The figure shows the detections in 3D detection space for saturation with a signal 30MHz above the radar signal band that saturates the amplifier and exhibits low spectral leakage.*

4.5.2 False detections from strong clutter

In this subsection false detections due to strong clutter that saturates the amplifiers, as seen to the right of figure 4.8, is treated. This is done in the same manner as the scenario with an external jammer in subsection 4.5.1. Since this section deals with the same waveform the clutter and target signal will be treated in the same way during the signal processing, which will facilitate the analysis of the signal.

Firstly the detection matrix for cases with 80% overlap between the echo and clutter is presented. In figure 4.23 the target is positioned behind the clutter source. The clutter is in the direction 135 deg azimuth while the target is at 60 deg.

As can be seen in figure 4.23 and 4.24 the clutter introduces quite a lot of false detections, albeit weak. The false detections that are strong enough also results in angular sidelobes. Observing figure 4.23 a ridge of false detections along the angle dimmension can be seen at the far side of the clutter main peak in the range dimension. This ridge share the doppler channel with the target, which also can be seen between the false detection ridge and the range bin for the main clutter peak, as illustrated in figure 4.23. At the same range as this ridge one can also observe a tower of weak false detections in the doppler dimension.

Most of these detections comes from the side lobes in range and angle dimension since the saturating clutter signal is sufficiently large so the tapering along the dimensions fail to fully suppress them with the used method. What is interesting to note is that the many false detection along the doppler dimension in the tower is positioned further away from both the pulse compressed target and the clutter echo. Another thing to note is that the ridge of false detections that appeared behind the target is positioned at the same doppler channel as that of the target, indicating that it relates to the velocity of the target and the overlap between the clutter and the target.

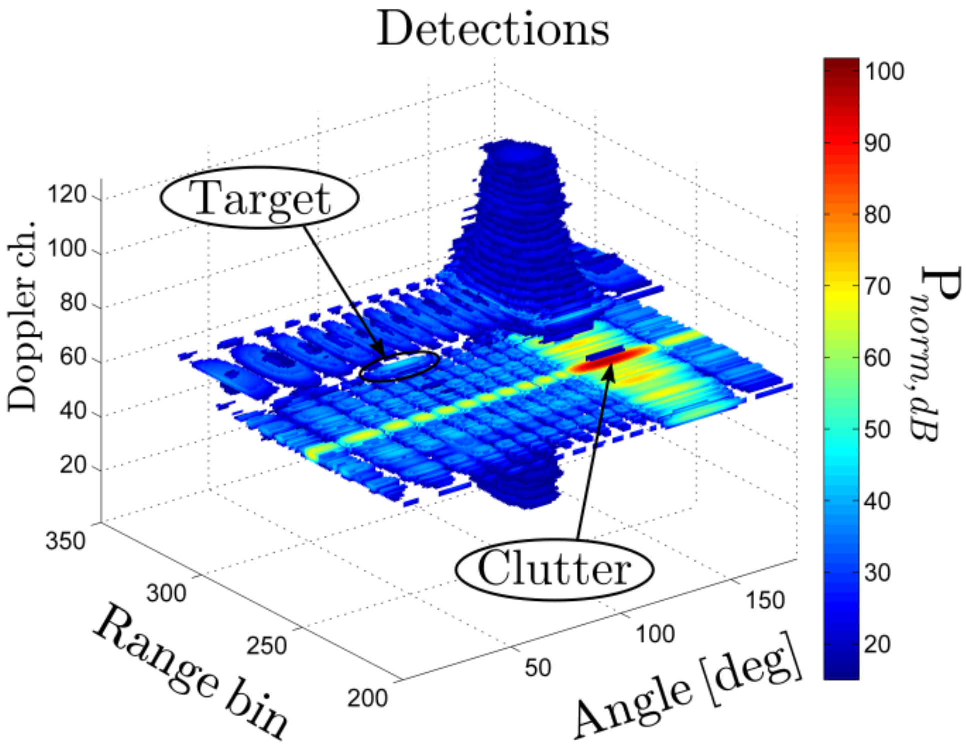

Figure 4.23: *The figure shows the detections in 3D detection space for saturation by a strong stationary (doppler channel 65) clutter signal at range bin 249 with a 80% overlap in time domain with the target echo. The target is positioned 19 range bins further away from the radar, at angle 60 degrees and has a radial velocity of -100m/s (doppler channel 76).*

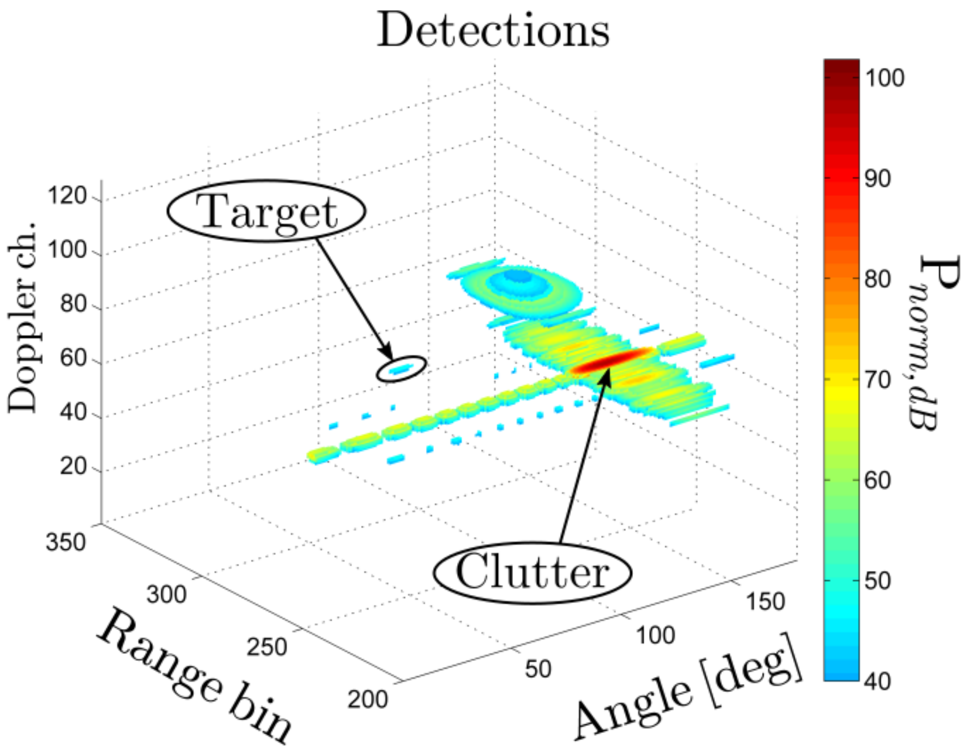

Figure 4.24: *The figure displays the same data as figure 4.23 but with a higher threshold for detection.*

By switching the distances of the target and clutter the detection matrix instead have the appearance showed in figure 4.25 and 4.26.

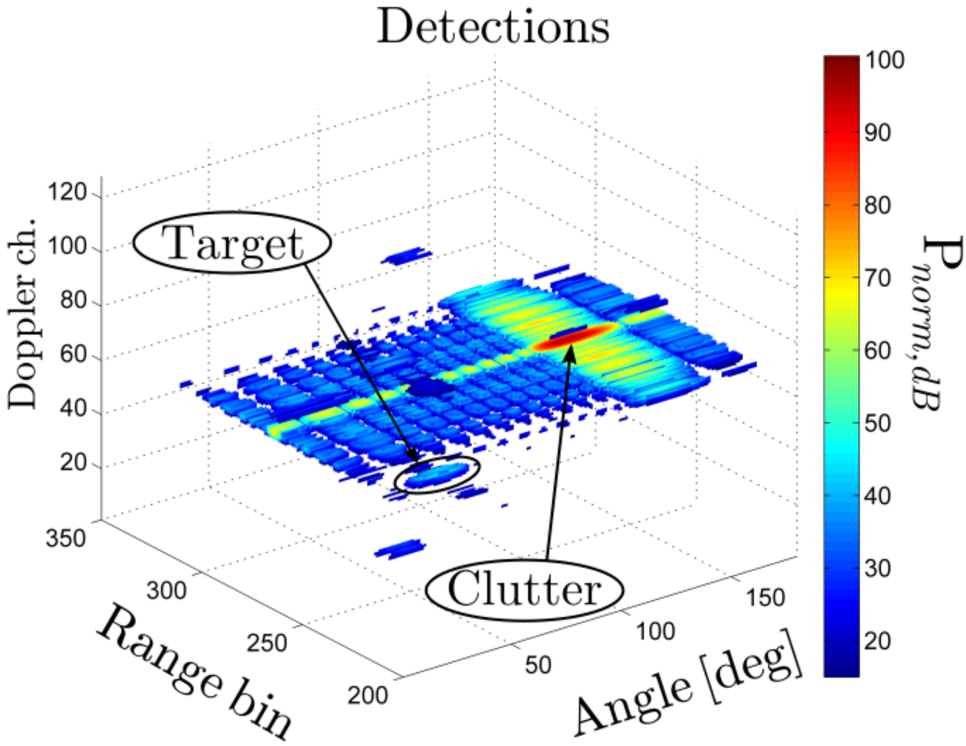

Figure 4.25: *The figure shows the detections in 3D detection space for saturation by a strong stationary (doppler channel 65) point clutter at range bin 255 with 80% overlap with the target echo. The target is positioned 19 range bins closer to the radar at angle 60 degrees, and has a radial velocity of -100m/s (doppler channel 76).*

Here the false detections has moved to the other side of the clutter peak and displays a more erratic, yet in doppler periodical, placement. The false detections at different doppler channels also becomes weaker in comparison with those of figure 4.23. They have also changed their appearances from having their centre at the direction of the clutter to that of the target echo, which is nearest.

This further illustrate that even if the overlap is the same, the order in which they reach the receiver greatly changes the appearance in the detection matrix. A further look into the placement of these false detections at different doppler channel is performed in subsection 4.5.3

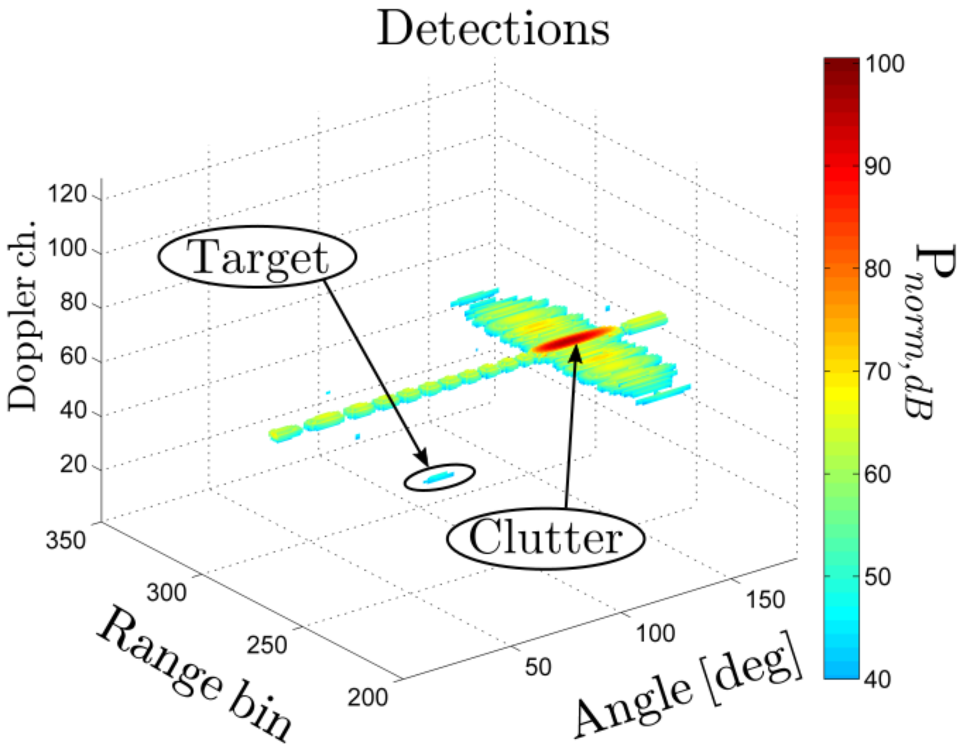

Figure 4.26: *The figure displays the same data as figure 4.25 but with a higher threshold for detection.*

4.5.3 False detection in doppler dimension

Having seen the general appearance of false detections from figures 4.23-4.26, in earlier subsections, this subsection strives to see how the false detections manifest at different positions and different target configurations. The scenario used is a strong clutter echo, overlapping the target echo with 100%, and the clutter echo is strong enough to saturate the amplifier. In this case study the point clutter is positioned with its maximum peak positioned at range bin 249 at direction 135 degrees azimuth, while the target comes from 60degrees.

Now since the clutter echo is strong enough to saturate the amplifiers and its power is being amplified in the same way as the target signal power the clutter will be strong enough so that the side lobes in the angle dimension appears above the threshold, as seen earlier in subsection 4.5.1 and 4.5.2. This is since ULA has rather few numbers of elements, which in turn leads to a lower side lobe suppression using tapering. This can be seen by observing the left part of figure 4.27 presenting the 2D cut at range bin 256 for a case when just the clutter is present. The reason for using range bin 256 instead of the range bin of the peak at 249 is that the false detections of interest doesn't appear at the correct clutter position but only in neighbouring range bins. From figure 4.27 it can also be seen that the side lobes indeed are about 30dB lower than the main peak, which is in accordance with the Taylor tapering described in section 2.4.1. Further on the clutter signal is also strong enough so that the side lobes from the doppler tapering appears round the main peak at 135 degrees, in accordance with the blackmann window [7].

By introducing a target with radial velocity -100m/s to the clutter situation the appearance of false detections are observed, as can be seen in figure 4.27b. One detection at an angle 60 degrees and doppler channel 76, corresponding to the target can be observed. Apart from this several detections at varying angle and doppler appears. As can be seen by comparing figure 4.27 and 4.28 the positions of these detections in doppler channel is linearly dependent of the velocity of the target where a doubling of the radial velocity of the target results in a shift in doppler channels from centre with a factor 2, and then the peaks fold around appearing at the opposite side.

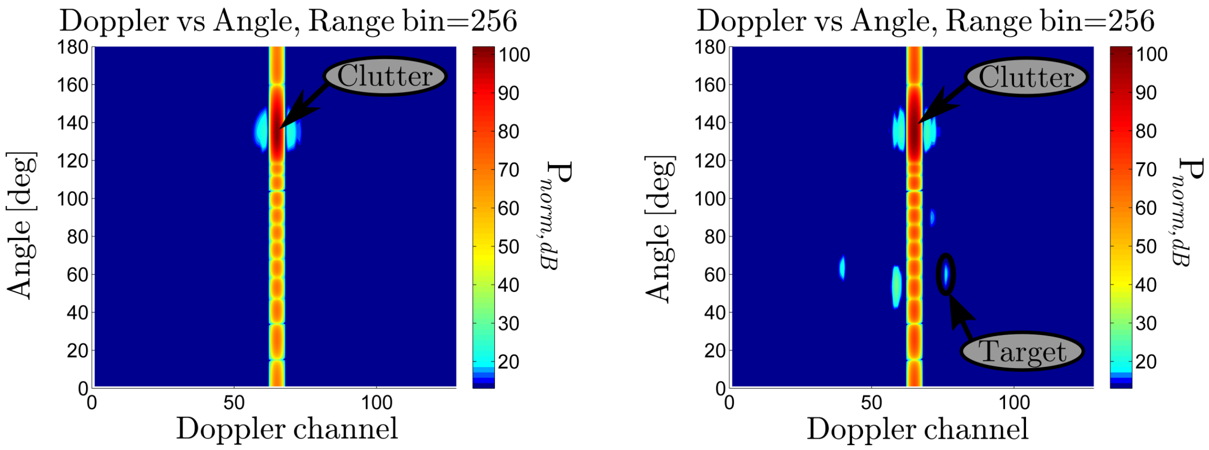

(a) (b)

Figure 4.27: *The figures shows doppler channel vs angle for a case with a target echo at direction 60deg in the presence of strong point clutter from 135deg. In the figure 4.27a the target is stationary (doppler channel 65), while in figure 4.27b the target has a radial velocity of -100m/s (doppler channel 76).*

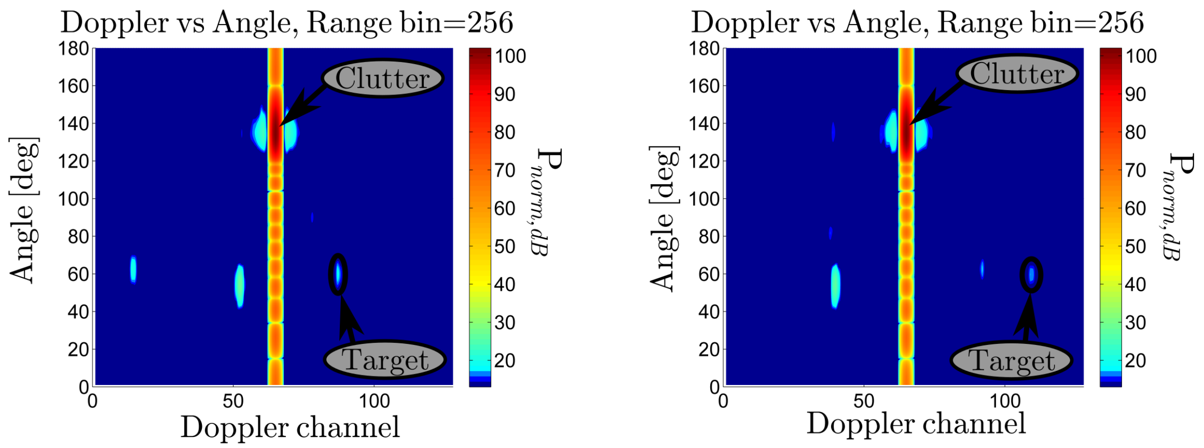

(a) (b)

Figure 4.28: *The figures shows doppler channel vs angle for a case with a target echo at 60 deg in the presence of strong stationary (doppler channel 65) point clutter at 135deg. In figure 4.28a the target has a radial velocity of -200m/s (doppler channel 87), while in figure 4.28b the radial velocity of the target is -400m/s (doppler channel 109).*

In the same way false detections can be observed at different range bins when observing in one specific direction. By observing figure 4.29 it can be seen that the clutter signal is strong enough that the side lobes from the pulse compression is visible even when observing in the direction of the target. In addition to this a false detection appears at a lower range bin, which also has some linear relation to the radial velocity of the target, which is the reason why the figures in 4.29 is mirrored.

These kind of false detection also appears at different directions than those of the target and disturbance and also manifest themselves when the clutter is switched to an external untapered jammer with centre frequency 50MHz higher then the transmitted signal. This is illustrated in figure 4.29. Here it can be seen that both the target and the jammer appears at their corresponding doppler channels even for directions separated from their real positions. As can be seen in figure 4.30 a strong peak appears in the direction of the jammer but at the doppler channel corresponding to the target velocity. This has its peak far below the expected range bin of the target and instead aligns with the jammer signal at lower range bins. This peak is also observed at different angles then those of towards both the target and the clutter as seen in figure 4.30b.

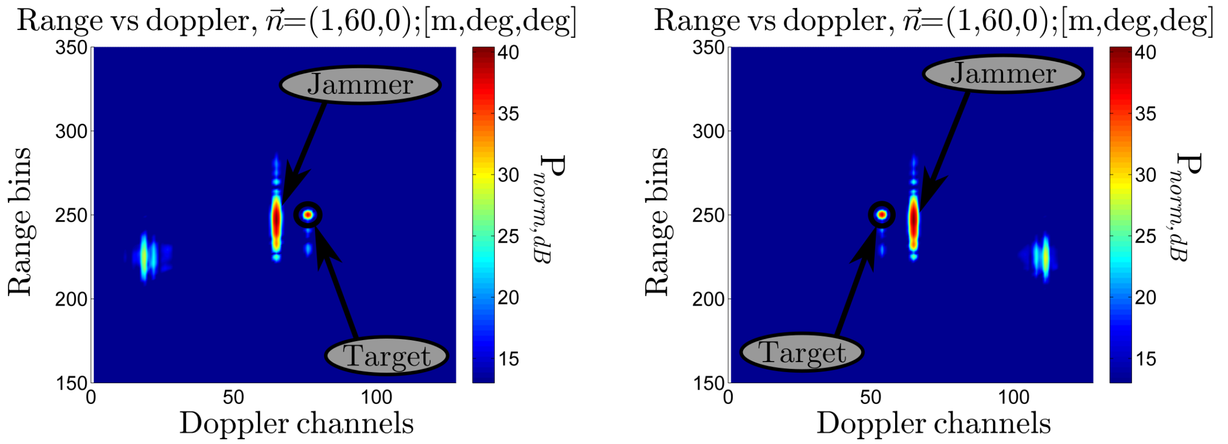

(a) (b)

Figure 4.29: *The figure shows range vs doppler channel for when a signal from a jammer at 90 deg overlaps a target echo with 93% at 60deg. The jammer transmits with the same PRF and band width as the radar but with a centre frequency 50MHz above that of the radar. Figure 4.29a has a target with radial velocity -100m/s (doppler channel 76), while 4.29a has a target with a radial velocity of 100m/s (doppler channel 54).*

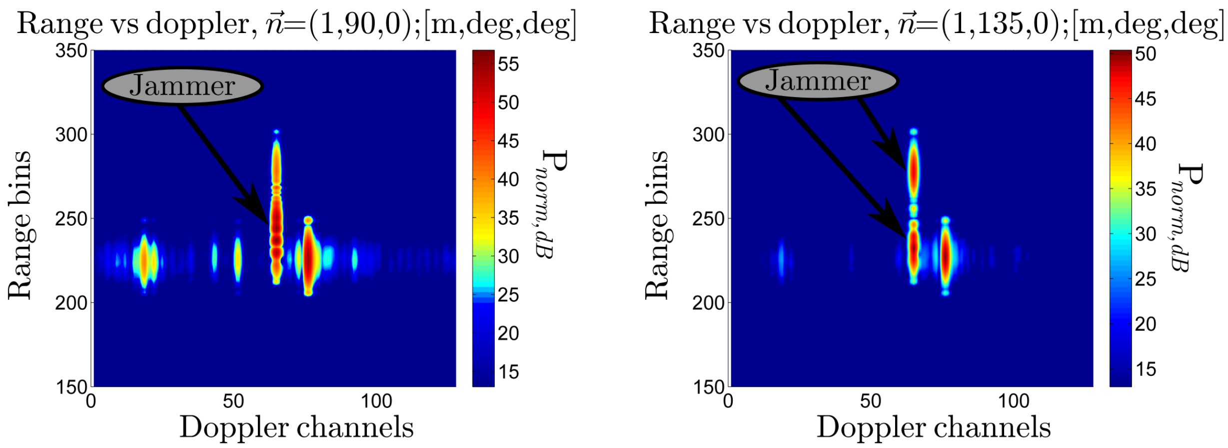

(a) (b)

Figure 4.30: *The figure shows range vs doppler channel for when the echo from a target is overlapped, by 93%, by an external jammer. The target has radial velocity -100m/s (doppler channel 76) positioned at range bin 249 in direction 60 degrees. The jammer has a centre frequency 50MHz above the radar signal and sends with a PRF equal to that of the radar at a direction from 135 degrees azimuth for figure 4.29a and 90 degrees for 4.29b.*

The results from these test continue to indicate the appearance of false detections along different doppler channels. These has a linear dependence of the velocity of the target, as seen by the fact that a increase of radial velocity also increases the perceived velocity of the false detections by the same amount. These false detections appears both at the same angle as the clutter and the target, but also at different angles without a clear relation, that can be discerned by scenarios simulated during this thesis.

5 Discussion

Looking at the results in chapter 4 it is seen that false detections appear when the signal becomes high enough so that the different side lobes starts appearing. Since the false detections are rather weak they should be susceptible to different kinds of counter measures that decreases the SNR of the jammer. This can be operations such that changing the window function for the tapering in order to improve the suppression. For cases when the doppler channel of the false detections are centred round 0 velocity ordinary clutter suppression techniques can be used. The straight forward way to decrease the side lobes in the angular dimension is through the increase of receiver elements, which makes better tapering possible. The tapering used for the beam forming in this theses only gives a side lobe suppression of 30dB. Another possibility is to change the tapering function so that a null is positioned in the direction of the clutter or jammer, which results in increased suppression.

For signals centred round a different centre frequency then the radar's frequency of operation there exists more alternatives. One way to suppress the external signal is through the use of a variable notch or band pass filter in the receiver circuit, capable of shifting which frequencies that should be suppressed. This also decreases the risk of saturating the amplifiers, at the cost of more hardware components.

When the problem lies in that the SNR of the desired echoes is lowered due to saturation of the amplifier as in section 4.3 or if the signal is clipped by the ADC such that the harmonics fold into the final band as described in section 2.5.1, one solution might be to attenuate the signal in the receiver before sampling with the ADC. The thought being to make sure the signal is attenuated so it isn't clipped by the ADC or to avoid compression in the amplifier, resulting in the non-linear behaviour. This has the effect that the attenuation might weaken already weak signals also present. A more software related approach, for situations containing an external jammer, that make use of the abilities of the broad band of the digital radar is to simply change the centre frequency of the transmitted signal and the band for the final sampling in order to avoid the frequency regions where an external signal is to strong. This doesn't avoid the saturation or the non-linearity but still constitutes a way to decrease false detections during operations, although still suffering the loss of SNR of the signal seen in figure 4.8. For saturated signal there's also the possibility to instead listen to band spanning the harmonics instead if one wants information about a particular strong signal.

Regarding the false detections that appears along the doppler dimension, these should be possible to treat during continuous observation. Given that the target under observation has one velocity but the false detections shows multiple, there should only be one detection that actually moves along the range dimension in accordance with the speed given by the doppler channel. The other false detection should not behave in this manner given that there exists no translation of this component in the time domain that would display the correct range behaviour.

When discussing the disturbance from external sources it is of interest to also look at recommendation regarding spectral leakage for commercial devices. These often has demand to operate within a spectral mask to avoid leakage outside their necessary bandwidth. These demands vary between regions but a typical spectral mask generated from the recommendations of ITU[18] are presented in figure 5.1.

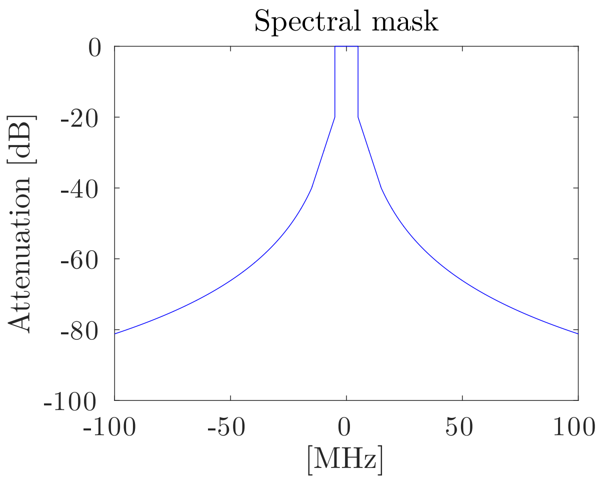

Figure 5.1: *The figure shows a spectral mask generated for a signal with 10MHz bandwidth using category A in ITU recommendation SM.329-12 (09/2012) [18]*

Had this mask been implemented in the case showed in figure 4.17 the leakage into the final sampling band would have been decreased, resulting in a situation like the one in figure 4.19.

6 Conclusion

In order to study the impact of replacing analogue filters in the radar receiver with digital filters a computational model for the radar system has been designed, that simulates the entire chain from signal generation to receiver and signal processing. This model has then been used to study cases where target echo overlaps with the clutter or external signals, which saturates the system.

The thesis found that saturation of the system negatively impacts the sensitivity and ability to discern a target due to decrease of the SNR when a different overlapping echo or external signal is strong enough to make the amplifiers go into compression. It also found that the saturation results in false detections when multiple signals overlap. These false detections has a linear relation to the radial velocity of the target in velocity space.

Further the thesis has treated the effect on detectability from an external jammer outside the radar signal band but inside the analogue filters of the receiver. It was found that it is indeed possible to suppress the signal outside of the sampling band digitally, but in the same way as for traditional radar even small spectral leakage into the band can be enough to generate false detections.

The thesis also states that the digital radar has large opportunity, unique to digital radar, to lessen the impact from external signals by varying the radar's centre frequency of operation and final sampling band in order to avoid frequency regions where external signals may fold.

Finally it states that performing full system simulations of a digital radar chain is feasible and gives the recommendation to perform experimental comparisons with the simulations and further study the behaviour and cause of the false detections, given rise to by the non-linearity, in order to better predict their behaviour.

References

[1] *AWRDE API Scripting Guide*. AWR Corporation. 2015. URL: `https://awrcorp.com/download/kb.aspx?file=docs/ApiReference.pdf`.

[2] *Behavioral Amplifier: AMP_B*. AWR Corporation, 2015. URL: `https://awrcorp.com/download/faq/english/docs/VSS_System_Blocks/AMP_B.htm`.

[3] C. Cattani and J. Rushchitsky. *Wavelet and Wave Analysis as Applied to Materials with Micro Or Nanostructure*. Series on advances in mathematics for applied sciences. World Scientific Publishing Company, 2007. ISBN: 9789812707840.

[4] *Component Object Model Technologies*. Microsoft, 2015. URL: `https://msdn.microsoft.com/library/ms680573%28VS.85%29.aspx`.

[5] *Compression Point*. Microwaves101, 2015. URL: `http://www.microwaves101.com/encyclopedias/compression-point`.

[6] G. B. Folland. *Fourier Analysis and Its Applications*. American Mathematical Society, 1992. ISBN: 978-0-8218-4790-9.

[7] F. Harris. On the use of windows for harmonic analysis with the discrete Fourier transform. *Proceedings of the IEEE* **66**.1 (1978), 51–83. ISSN: 0018-9219. DOI: `10.1109/PROC.1978.10837`.

[8] *HDF5*. The HDF Group, 2015. URL: `https://www.hdfgroup.org/HDF5/`.

[9] J. D. Jackson. *Classical Electrodynamics*. 3rd ed. John Wiley & Sons, 1999.

[10] J. B. Johnson. Thermal Agitation of Electricity in Conductors. *Phys. Rev.* **32** (1 1928), 97–109. DOI: `10.1103/PhysRev.32.97`. URL: `http://link.aps.org/doi/10.1103/PhysRev.32.97`.

[11] R. Mailloux. *Phased Array Antenna Handbook*. 2nd ed. Artech House, 2005. ISBN: 9781580536905.

[12] *MAT-file Versions*. Mathworks. 2015. URL: `https://se.mathworks.com/help/matlab/import_export/mat-file-versions.html#responsive_offcanvas`.

[13] D. M. Pozar. *Microwave Engineering*. 4th ed. John Wiley & Sons, Inc, 2012. ISBN: 978-0-470-63155-3.

[14] *Principles of Data Acquisition and Conversion*. Texas Instruments. 2015. URL: `www.ti.com/lit/an/sbaa051a/sbaa051a.pdf`.

[15] *Saturated output power*. Microwaves101, 2015. URL: `http://www.microwaves101.com/encyclopedias/power-amp-designer101`.

[16] D. V. Schoeder. *Thermal Physics*. Addison Wesley Longman, 2000. ISBN: 0-321-27779-1.

[17] M. I. Skolnik. *Radar Handbook*. 3rd ed. McGraw-Hill Professional, 2008.
[18] *SM.329 : Unwanted emissions in the spurious domain*. ITU, 2012. URL: https://www.itu.int/rec/R-REC-SM.329-12-201209-I/en.
[19] MATLAB®. Mathworks, 2015. URL: https://se.mathworks.com/products/matlab/.
[20] *The relationship of intercept points composite distortions and noise power ratios*. Matrix Technical Notes MTN-109. Matrix test equipment incorporated, 2010. URL: http://www.matrixtest.com/FILES/mtn109.pdf.
[21] *VSS*. AWR Corporation, 2015. URL: http://www.awrcorp.com/products/visual-system-simulator.
[22] *Windows Powershell Owner's Manual*. Microsoft. 2015. URL: https://technet.microsoft.com/en-us/library/ee221100.aspx.
[23] W.-D. Wirth. *Radar Techniques Using Array Antennas*. 2nd ed. The Institution of Engineering and Technology, 2013. ISBN: 978-1-84919-698-7.

Fifth order 2-tone expansion coefficients

Table 1

cos	$A\cos(\omega_1 t)+B\cos(\omega_2 t)$	$(A\cos(\omega_1 t)+B\cos(\omega_2 t))^2$	$(A\cos(\omega_1 t)+B\cos(\omega_2 t))^3$	$(A\cos(\omega_1 t)+B\cos(\omega_2 t))^5$
DC		$\frac{A^2+B^2}{2}$		
ω_1	A		$\frac{3A^3+6AB^2}{4}$	$\frac{10A^5+30AB^4+60A^3B^2}{16}$
ω_2	B		$\frac{3A^3+6AB^2}{4}$	$\frac{10A^5+30AB^4+60A^3B^2}{16}$
$2\omega_1$		$\frac{A^2}{2}$		
$2\omega_2$		$\frac{B^2}{2}$		
$3\omega_1$			$\frac{A^3}{4}$	$\frac{5A^5+20A^3B^2}{16}$
$3\omega_2$			$\frac{B^3}{4}$	$\frac{5B^5+20A^2B^3}{16}$
$5\omega_1$				$\frac{A^5}{16}$
$5\omega_2$				$\frac{B^5}{16}$
$\omega_1+\omega_2$		AB		
$\omega_1-\omega_2$		AB		
$2\omega_1+\omega_2$			$\frac{3A^2B}{4}$	$\frac{20A^4B+30A^2B^3}{16}$
$\omega_1+2\omega_2$			$\frac{3AB^2}{4}$	$\frac{20AB^4+30A^3B^2}{16}$
$2\omega_1-\omega_2$			$\frac{3A^2B}{4}$	$\frac{20A^4B+30A^2B^3}{16}$
$\omega_1-2\omega_2$			$\frac{3AB^2}{4}$	$\frac{20AB^4+30A^3B^2}{16}$
$3\omega_1+2\omega_2$				$\frac{10A^3B^2}{16}$
$2\omega_1+3\omega_2$				$\frac{10A^2B^3}{16}$
$3\omega_1-2\omega_2$				$\frac{10A^3B^2}{16}$
$2\omega_1-3\omega_2$				$\frac{10A^2B^3}{16}$
$4\omega_1+\omega_2$				$\frac{5A^4B}{16}$
$\omega_1+4\omega_2$				$\frac{5AB^4}{16}$
$4\omega_1-\omega_2$				$\frac{5A^4B}{16}$
$\omega_1-4\omega_2$				$\frac{5AB^4}{16}$